Design of Particle swarm optimized Two-Degree-of-Freedom PID Controllers for Automatic Load Frequency Control of Two area Hydro-Hydro Power Plants

Abraham Tsige Tegegn

A Thesis Submitted to

The Department of Electrical Power and Control Engineering

School of Electrical Engineering and Computing

Office of Graduate Studies

Adama Science and Technology University

May, 2024

Adama, Ethiopia

Design of Particle swarm optimized Two-Degree-of-Freedom PID Controllers for Automatic Load Frequency Control of Two area Hydro-Hydro Power Plants

Abraham Tsige Tegegn

Advisor: Dr. Endalew Ayenew

A Thesis Submitted to

The Department of Electrical Power and Control Engineering
School of Electrical Engineering and Computing

Office of Graduate Studies
Adama Science and Technology University

May, 2024

Adama, Ethiopia

DECLARATION

I hereby declare that this Master Thesis entitled "Design of Particle Swarm Optimized Two-Degree-of-Freedom PID Controllers for Automatic Load Frequency Control of Two area Hydro-Hydro Power Plants" is my original work. That is, it has not been submitted for the award of any academic degree, diploma, or certificate in any other university. All sources of materials that are used for this thesis have been acknowledged through citation.

Abraham Tsige	____________________	________________
Name of student	Signature	Date

RECOMMENDATION

I, the advisor of this thesis, hereby certify that I have read the revised version of the thesis entitled "Design of Particle Swarm Optimized Two-Degree-of-Freedom PID Controllers for Automatic Load Frequency Control of Two area Hydro-Hydro Power Plants" prepared under my guidance by Abraham Tsige Tegegn submitted in partial fulfillment of the requirements for degree of Masters of Science in Control Engineering. Therefore, I recommend the submission of a revised version of the thesis to the department following the applicable procedures.

___Dr. Endalew Ayenew_	____________________	______________________
Advisor	Signature	Date

APPROVAL PAGE

I, the advisor of the thesis entitled "Design of Particle Swarm Optimized Two-Degree-of-Freedom PID Controllers for Automatic Load Frequency Control of Two area Hydro-Hydro Power Plants" and developed by Abraham Tsige Tegegn hereby certify that the recommendation and suggestions made by the board of examiners are appropriately incorporated into the final version of the thesis.

Dr. Endalew Ayenew	____________________	____________________
Advisor	Signature	Date

We, the undersigned, members of the Board of Examiners of the thesis by Abraham Tsige Tegegn have read and evaluated the thesis entitled "PSO-based Two-Degree-of-Freedom PID Controllers for Automatic Load Frequency Control of Two Area Hydro-Hydro Power Plants" and examined the candidate during the open defense. This is, therefore, to certify that the thesis is accepted for partial fulfillment of the requirement of the degree of Master of Science in Control Engineering.

____________________	____________________	____________________
Chair Person	Signature	Date
____________________	____________________	____________________
Internal Examiner	Signature	Date
Dr. Riessom Weldegiorgis	[signature]	30/06/2024
External Examiner	Signature	Date

Final approval and acceptance of the thesis is contingent upon submission of its final copy to the Office of Postgraduate Studies (OPGS) through the Department Graduate Council (DGC) and School Graduate Committee (SGC).

____________________	____________________	____________________
Department Head	Signature	Date
____________________	____________________	____________________
School Dean	Signature	Date
____________________	____________________	____________________
Office of Postgraduate Studies, Dean	Signature	Date

ACKNOWLEDGEMENTS

First and foremost, I would like to express my deepest gratitude to my God for providing me with the knowledge, strength, and persistence to undertake and complete this thesis. Without his guidance and blessing, this thesis would not have been possible.

I would also like to extend my sincere appreciation to my advisor, **Dr. Endalew Ayenew**, for his unwavering support, invaluable insights, and continuous encouragement throughout my work. His experience, patience, and mentorship have been instrumental in shaping this thesis.

I am also grateful to **Professor Gang Gyoo Jin**, whose valuable feedback, collaborative spirit, and intellectual contribution have been crucial in refining and enriching the content of this thesis. Your willingness to share your knowledge and expertise has been truly appreciated.

I am eternally grateful to my beloved wife, **Sifen Abebe**, for her unconditional love, endless patience, and unwavering support throughout this endeavor. Your understanding and willingness to make sacrifices have been a constant source of strength and inspiration. I would also like to express my deepest love and appreciation to my darling daughter, **Melona Abraham**, who has brought immeasurable joy and purpose to my life during this challenging journey.

Furthermore, I am grateful to my friends, **Mr. Gera Worku and Mr. Desalegn Tegegn**, for their support and valuable discussion, and feedback that have enriched my research experience.

Finally, I extend my heartfelt gratitude to my family and loved ones for their unconditional love, understanding, and support during the countless hours spent on this endeavor. Your unwavering encouragement has been a constant source of motivation and inspiration.

Thank you all for your contributions, both big and small, that have made the completion of this thesis possible.

CONTENTS

LIST OF TABLES

LIST OF FIGURES

LIST OF ACRONYMS

ACE	Area Control Error
AGC	Automatic Generation Control
ALFC	Automatic Load Frequency Control
ANN	Artificial Neural Network
AVR	Automatic Voltage Regulation
BFA	Bacteria Foraging Algorithm
EA	Evolutionary Algorithm
EEP	Ethiopian Electric Power
FACTs	Flexible AC Transmission Systems
FLC	Fuzzy Logic Control
GERD	Grand Ethiopian Renaissance Dam
HEPP	Hydro-Electric Power Plant
HVDC	High Voltage Direct Current
IAE	Integral Absolute Error
ISE	Integral Square Error
ITAE	Integral Time Absolute Error
ITSE	Integral Time square Error
LDC	Load Dispute Center
LFC	Load Frequency Control
LQR	Linear Quadratic Regulator
MPC	Model Predictive Control
PI	Proportional Integral
PID	Proportional Integral Derivative
PSO	Particle Swarm Optimization
RFB	Redox Flow Battery
TDOF-PID	Two Degree-Of-Freedom PID
UC	Ultra-Capacitor

ABSTRACT

In power systems that are interconnected, any sudden small load change in any of the power systems in the interconnected grid causes the deviation of tie-line power and area frequency. Automatic Load Frequency Control (ALFC) plays a very important role in Automatic Generation control (AGC) to maintain system frequency and active power flow at their scheduled values during any load perturbation. In this thesis, a two-degree-of-freedom proportional-integral-derivative (TDOF-PID) controller is proposed and successfully applied for ALFC of two interconnected hydropower systems. The objective is to control the frequency deviation by maintaining the real power balance using the TDOF-PID controller. The TDOF-PID controller, integrated with a particle swarm optimization algorithm, effectively addresses the issues of frequency deviation and tie-line power deviation, which have a significant impact on power system stability and quality. The TDOF-PID controller has demonstrated exceptional performance in managing the power balance and maintaining system stability in the two-area interconnected hydropower system. Compared to an uncontrolled system, the TDOF-PID-PSO controller exhibits remarkable improvements across various metrics. It exhibits extremely low Integral Absolute Error (IAE) and Integral Time Absolute Error (ITAE) values, even for large 20% load changes in either area, indicating excellent load disturbance rejection capabilities. The frequency deviations in both areas are kept to a minimum, with changes in the range of -0.02 Hz to -2.03 Hz, even for the 20% load changes, which is within the acceptable frequency range according to Ethiopian Electric Power for power quality and system reliability. The controller also demonstrates effective management of the tie-line power exchange between the two areas, with a maximum tie-line power deviation of only 0.086 per unit, even for large disturbances. In addition to stability and reliability, the TDOF-PID-PSO controller shows promise in terms of economic dispatch and efficiency, as indicated by the low IAE and ITAE values. The controller's performance remains consistent and effective under both small (1%) and large (20%) load changes, demonstrating its robustness and adaptability. It is concluded that the TDOF-PID-PSO controller has proven to be an exceptional solution for managing the tie-line power balance and ensuring the stability and reliability of the two-area interconnected hydropower system. Its sophisticated control strategies and adaptability make it a highly recommended solution for this critical power system application

Key words: AGC, ALFC, Interconnected hydropower, load perturbation, PSO, TDOF-PID.

CHAPTER ONE

INTRODUCTION

1.1 Background of the study

The need for electricity is growing every day for a variety of reasons, and the power system is evolving quickly to meet system requirements while delivering electricity efficiently despite various operational constraints. To operate the system reliably and economically, the electrical power system was networked. To meet the demand, the generation power should also rise (Joshi et al., 2023). Ethiopia with a peak load of 4800 MW and an installed generation capacity of approximately 5,256.5 MW, hydropower accounts for the greatest share of Ethiopia's energy output, accounting for 91% (4820.2 MW) of the total installed capacity and 93,4% of annual electricity production. (https://www.eep.com.et/?page_id=1033).

The nation's strong industrial and economic growth has led to a progressive increase in the overall load and the expansion of the nation's power infrastructure.(Mondal et al., 2018). Nevertheless, the nation finds it challenging to meet the power demand due to different reasons. The first and most difficult reason in this regard is the mismatch of the load perturbation which is caused by different causes.

Both the system frequency and the AC tie-line power deviated due to the imbalance between the generation of electric energy and the consumption of load, resulting in an unacceptable value. Deviations from ideal power quality and consistent electricity delivery to customers can occur. To address this, modern power systems rely on Automatic Generation Control as a core element of secondary frequency control. This technology maintains the system's frequency near its planned level (Kiviluoma et al., 2016). In which the AGC system has two parts which are the Load frequency control used to control the Active power (P) and the frequency (F) of the system, and the Automatic voltage regulation that controls the relationship between the reactive power (Q) and Voltage (V) (More Raju, n.d.).

The Automatic Load Frequency Control helps maintain stability by minimizing deviations in both frequency and power exchange with neighboring areas (tie-line power). This is achieved by keeping the Area Control Error (ACE) close to zero. The ACE is a metric that combines the system’s frequency deviation and the change in tie-line power, essentially representing the net difference between power generation and demand within a specific control zone (Joshi et al., 2023). This mismatch makes the power systems unstable. As a result, acceptable bounds must be maintained for scheduled frequency and tie-line powers. Automatic load frequency control requires power system controllers to be built in a way that controls power flow between tie lines and frequency in connected areas (More Raju, n.d.). ALFC makes area control error zero to keep frequency and tie-line power within a preset range.(Kundur & Malik, n.d.-a).A generation area has to generate more energy overall if its ACE is negative; conversely, if its ACE is positive, it needs to reduce production since it is overproducing. ALFC is made up of a feedback control loop that optimizes transient behavior while adjusting the frequency within bounds to produce zero steady-state faults. While variations in reactive power are more sensitive to changes in frequency, variations in actual power primarily affect the system frequency and vice versa. Therefore, reactive and Active powers are managed differently.

The power customers have been directly impacted by operating point changes due to the growing non-linearity and complexity of power systems, raising concerns regarding power quality.(Kundur & Malik, n.d.-a). In numerous interconnected locations, any fault, interruption, or disruption can negatively impacts the power quality of the power system.(More Raju, n.d.). conversely, an interconnected power system consists of a single, bulky electric circuit that has historically been divided into control areas. Every control area usually corresponds to a single power production component of the interconnected power system. These separate areas are interconnected via a tie line to interchange the net power flow out of a specific control area. Thus, by interconnecting different power systems including the old plants we can improve the efficiency, reliability, and cost-effectiveness of the power system.

In the case of hydroelectric power generation, the water supplied from the reservoir through the penstock into the turbine must be adjusted continuously to satisfy the need of the active power otherwise, the turbine speed will alter and consequently, the frequency deviates in an unmannered way (Masuta & Yokoyama, 2012) Correspondingly, the reactive power must be balanced with the reactive generation using the excitation system to overcome the overvoltage faults (Aung & Htike, n.d.2019). However, frequency control takes precedence over voltage control (Patrick et al., 2022). Consequently, regulation of the interconnected power system is very concerning. In today's large-scale interconnected power system manual regulation is impossible. So, each alternator must have an automatic frequency and voltage-controlling mechanism namely Automatic load frequency control and automatic voltage regulator respectively. These controllers are configured for a specific application and handle a tiny fluctuation in load demand without exceeding the frequency limit. Thus, to improve these problems the secondary loop in the governing system of the generation with PID controller is the most known method applied to ALFC for its feasibility (G. Shankar & Mukherjee, 2016). 1DOF-PID controllers have set parameters, making them unsuitable for the complexity and nonlinearities of interconnected power systems; specially in hydropower systems due to the water column nonlinearity nature today's hydropower plants use PID controllers only for isolated power systems. As a result, in several studies, the TDOF PID (two degrees of freedom proportional integral derivative), (Sahu et al., 2013) controllers were used

Thus, this thesis is a study of ALFC in two areas (hydro and hydro) interconnected power systems considering the interruption that happened in Ethiopia's electric system. The study chooses two interconnected hydroelectric power plants in Ethiopia (Koka hydroelectric power plant and Awash II and III power plants) as an input; by focusing on tuning the 2DOF PID controller to get the optimum values of the parameters which reduces area control error to get the stable frequency and tie-line power.

1.2 Statement of the problem

Modern power grids experience frequency deviations when load changes because of how generators and loads interact. Regardless of where a load change occurs, all generators with speed control contribute to the overall frequency shift due to their droop characteristics and load frequency sensitivity. In real-world operation, constant and unpredictable load variations challenge generators' ability to perfectly match demand. This mismatch between actual and scheduled generation creates a "frequency error," the difference between the actual frequency and the ideal synchronous frequency. This unbalance between the generation quantities led the power system to different power failures. In Ethiopia, there was a repetition of power interruptions that led the power system to partial and total blackouts of power. These power interruptions happened at different times with different loads for the same reason; under frequency. Recently on March 28, 2024, and July 11, 2023, with a fault record of under frequency of the system due to Gilgel gibe III HEPP Auxiliary outage and GERD-Dedesa line outage respectively. Those faults happened with the same frequency of 47.11 Hz which is under the nominal frequency range of EEP. Due to these two problems, the country lost an energy of 10671.88 MWA and 12287.94 MWH respectively. The study proposes using a TDOF (Two

Degrees of Freedom) PID controller as a solution to address the problems outlined previously. The TDOF PID controller is designed to effectively manage the frequency deviations and the frequency error in the power system, thereby improving the overall stability and reliability of the grid. The validation for the blackout is attached in the Appendix.

1.3 Objective of the Thesis

1.3.1 General objective:

The general objective of this thesis is to design a PSO-optimized two-degree-o-freedom PID controller to control the frequency deviation by maintaining the real power balance between two area hydroelectric power plants and simulate the power regulation capability under load disturbances.

1.3.2 Specific Objectives:

- To drive the mathematical model of a hydro-hydropower system.
- To design PSO-based TDOF PID controllers
- To simulate the overall system result using MATLAB/Simulink with TDOF PID controller's implementation.
- To perform frequency deviation analysis on interconnected power systems under different load disturbances.

1.4 Scope and Limitation of the thesis

This thesis involves the study and design of the optimal control of automatic load frequency control for hydropower systems. An optimization strategy will be applied to obtain the two-degree-of-freedom proportional-integral-derivative controller parameters and the simulation will be developed using MATLAB/ Simulink.

1.5 The Motivation of the Study

Demand for power consumption rises in tandem with population growth and industrialization. A rise in demand results in a variety of loads. As a result, there is a discrepancy between load demand and power supply since load demand fluctuates constantly. This discrepancy has made frequency management a serious issue. Power systems are sensitive to fluctuations in electrical demand, which we cannot directly control or perfectly predict. This makes it challenging to take corrective actions immediately. To address this, an error signal called Area Control Error (ACE) is calculated based on both the system's frequency deviation and the power exchanged between control areas. This research proposes using a controller with optimized settings determined by a metaheuristic optimization algorithm. The goal is to minimize the ACE and improve overall system performance.

1.6 Significance of the Study

Stable electrical grids rely on precise control of power frequency. Since fluctuations in active power cause frequency variations, Maintaining the scheduled system frequency is of critical importance in electrical power systems. Deviations in frequency are directly caused by imbalances in the active power of the network. Implementing an automatic load frequency control mechanism can be used to govern and regulate these frequency variations. Thus the primary contribution of this thesis work is to investigate and propose an appropriate controller design for automatic load frequency control in a hydropower system with tie-line interconnections. The goal is to develop a controller that can effectively manage the frequency deviations and ensure the reliable operation of the power system

1.7 Organization of the Thesis

This thesis is structured into four distinct chapters, and a conclusion and recommendation part.

Chapter 2: Consists of a literature review on the Automatic load frequency control, the controller used, single-area power system, and two-area power system areas.

Chapter 3: Outlines the materials used and the methodologies followed in conducting the thesis.

Chapter 4: presents the results and provides a detailed discussion of the findings.

Finally, the conclusions and recommendations of the thesis.

CHAPTER TWO

LITERATURE REVIEW

2.1 Automatic Load Frequency Control (ALFC)

In large-scale electrical networks, frequency instability is a significant concern and a significant challenge for operators of the power supply. Oscillation frequency issues have proliferated along with the expansion of linked power networks, raising the possibility of complete blackout, zone isolation, multiple line losses, and disconnection measures. Since the operating points are always changing, stabilizing the scheduled power exchange has always been challenging, even though it is managed by local generation dispatch rather than automatic control (Joshi et al., 2023a). This perception makes the feasibility of Automatic load frequency Control apparent. As important functions of AGC, power system frequency and voltage regulation have been one of the big challenges in interconnected electrical networks.

The growing scale and interconnectedness of power grids necessitate a renewed focus on maintaining system stability. This translates to a heightened emphasis on ALFC and AVR strategies. Real-world power systems often encompass numerous interconnected areas, frequently exhibiting similar characteristics across these areas. Considering this practical scenario, this thesis adopts a simplified model of a two-area power system, each containing two hydroelectric generating units. This choice allows for a focused exploration of control strategies while maintaining a level of complexity that reflects real-world systems.

In ensuring the reliable operation of interconnected power systems, separate control mechanisms are crucial for managing frequency and voltage. ALFC focuses on maintaining system frequency by regulating active power, while AVR keeps voltage levels stable by adjusting reactive power. LFC has garnered significant research interest in recent years due to the importance of active power-frequency control compared to reactive power-voltage control. This emphasis stems from the inherent inertia of rotating machinery in power plants, which helps buffer frequency deviations caused by active power imbalances (Hanwate et al., 2018).

A load frequency controller is utilized to control an error signal, taking into consideration inaccuracies in the interconnected system frequency (Δf) or inaccuracies in the interchange power with nearby regions linked by tie lines.

Ensuring a reliable and high-quality power supply is crucial for any power system. Here's where LFC comes in. Manually managing a large-scale power system is impossible, so each generator relies on automatic generation and voltage control equipment. These controllers can handle minor load fluctuations without affecting frequency limits. However, for significant load changes, the controllers may need to be readjusted, either manually or automatically. In general, these automatic controllers play a vital role in maintaining both the frequency (active power) and voltage (reactive power) within a power system.

This research investigates the application of a TDOF PID controller to achieve frequency stability in a power system. The focus is on mitigating the impact of sudden changes in load demand (step load disturbances) on system frequency.

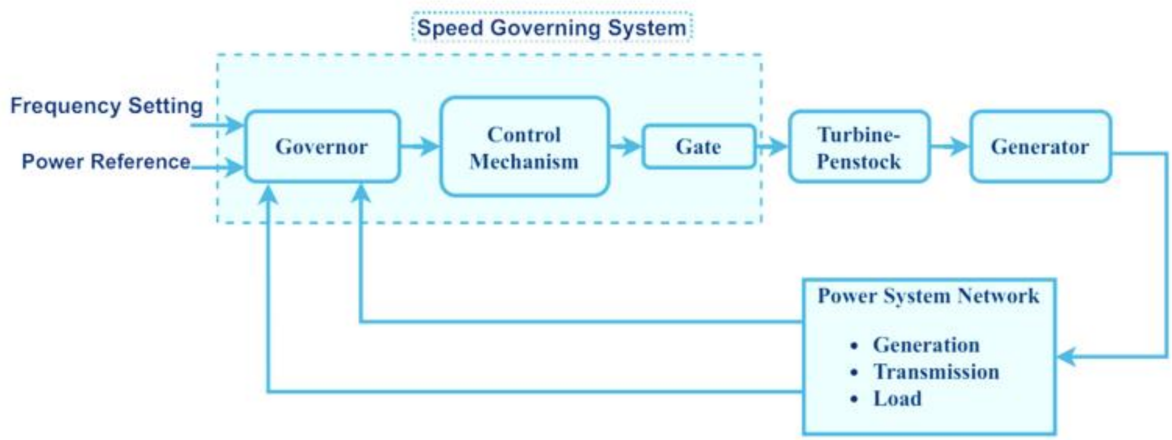

Figure 2.1 Block diagram representation of the ALFC technique (Fardo & Patrick, n.d.)

2.2 Automatic Load Frequency Control of Single Area Power System

In a power system, the ALFC acts as a conductor's baton, ensuring everything stays in tune. It achieves this by maintaining a real power balance, essentially keeping supply and demand in sync. This allows the ALFC to fulfill its key functions: holding system frequency steady, managing the flow of power between interconnected areas, and distributing the load efficiently among participating generators (Kundur & Malik, n.d.-a). To maintain power balance, the system monitors both frequency deviation (obtained from angle deviation) and tie-line power flow deviation. These error signals are amplified, combined, and converted into a control signal that adjusts the valve position. This, in turn, directs the turbine (primary mover) to modify its output power. (Patrick et al., 2022). Figure 2.2 depicts the Schematic diagram of a single-area ALFC system.

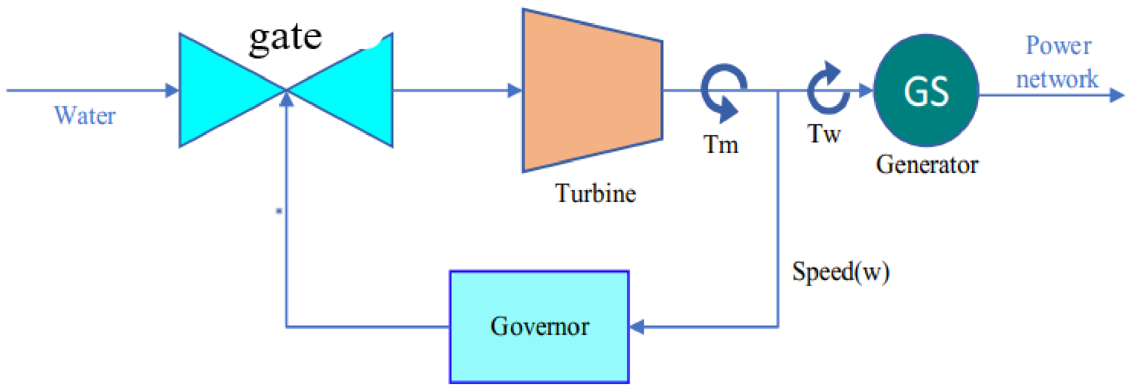

Figure 2.2 The Schematic diagram of a single-area ALFC system (Kundur & Malik, n.d.-b)

2.3 Interconnected Power System

Practically speaking, issues with frequency and voltage regulation in interconnected areas are more significant than those in isolated or single areas as shown in the figures below which describe the advantage of an interconnected area over an isolated power system using the data from two power plants in Ethiopia.

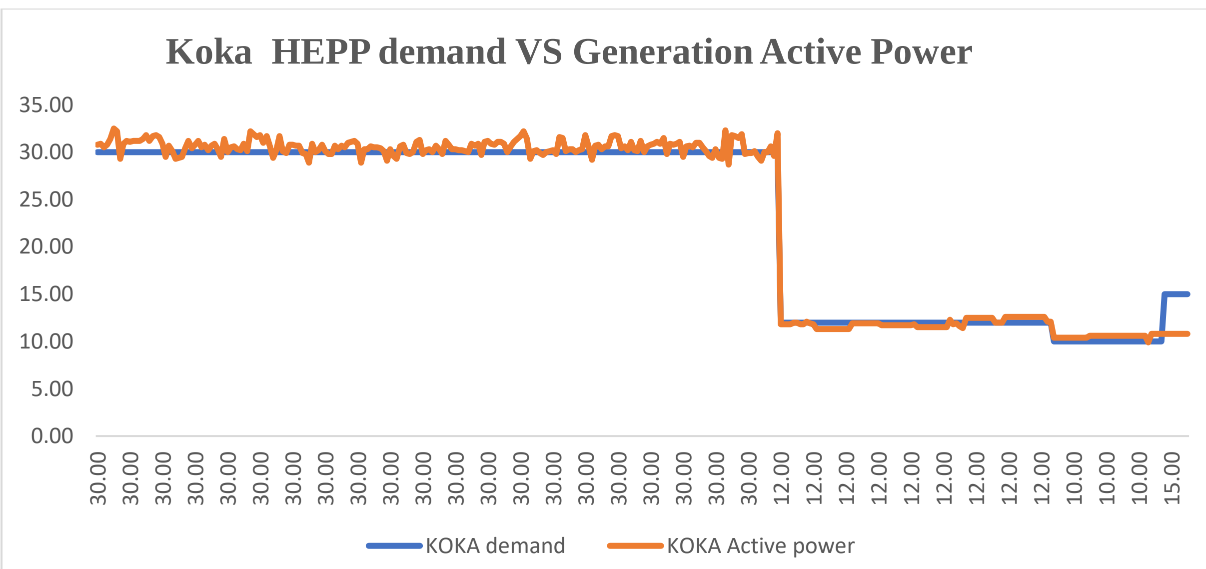

(a)

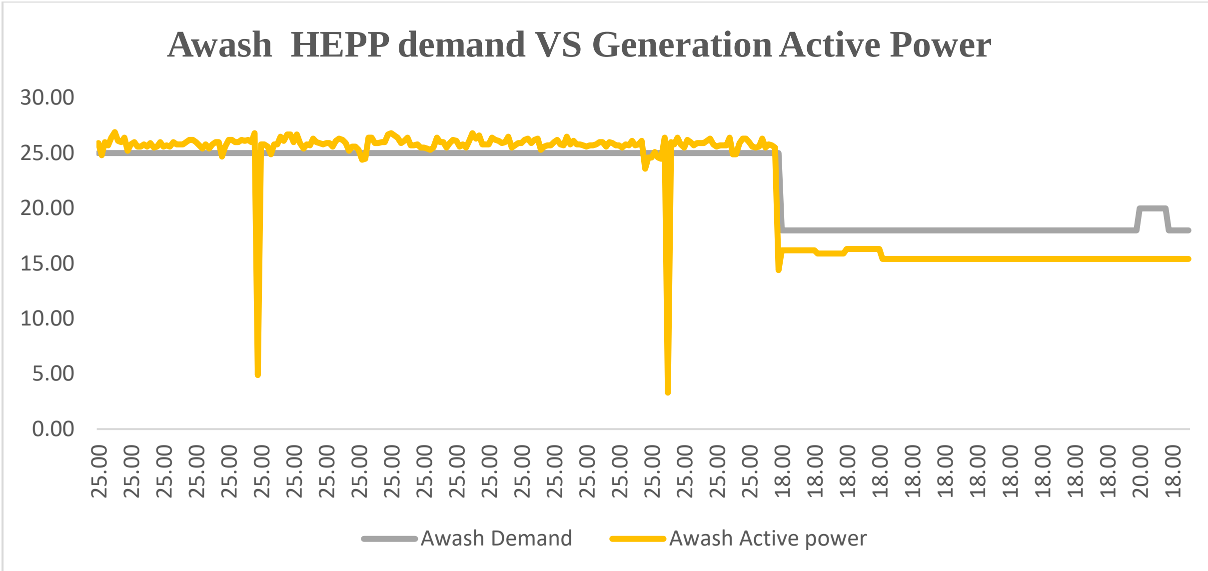

(b)

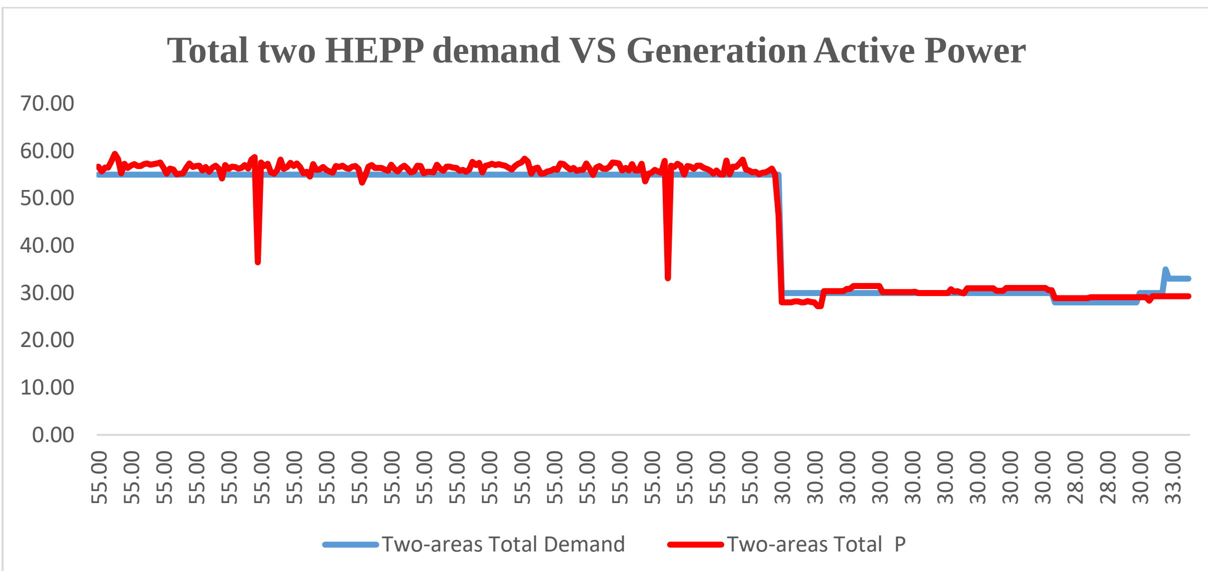

(c)

Figure 2.3 Active generation power vs demand (a) Koka HEPP, (b) Awash II and III HEPP, and (c) combined two area system

Here in Figure 2.3, we have seen the advantage of an interconnected system over a single-area system to satisfy the power demand. In Figure 2.3 a and b, the demand and the generated power are not a good match for a single area whereas, for an interconnected system, they share their load to some extent to match the demand and the generating power. While focusing on multi-area systems offers valuable insights into complex interconnected power grids, grasping the fundamental theory and concepts behind single-area control systems remains crucial. This foundational knowledge serves as a springboard for understanding the interactions and challenges that arise when multiple areas are interconnected. Nowadays autonomous generation control is a problem since almost all power systems in existence are interconnected with nearby regions. (Chand Bansal et al., n.d.2017)

Benefits of Interconnected power system:

- Economy of Scale: The larger the interconnected system, the greater the benefit of "economy of scale." When a new load is added to the system, it can temporarily draw on the kinetic energy stored in the rotating machinery across the entire network. Larger systems inherently have more available energy to meet such demands.
- Reduced Reserve Requirements: Larger interconnected systems experience a smaller ratio of peak load to average load compared to smaller, isolated systems. This is because peak demands tend to occur at different times in different geographical locations. By sharing reserves across the interconnected system, the overall reserve capacity requirement is reduced compared to the sum of individual reserves needed for isolated operation

A scheduled plan for energy interchange among interconnected areas can demonstrably reduce the overall reserve capacity requirement for each area (Liu et al., 2023).

Hydroelectric power generation faces several challenges related to ALFC. Here are some key issues.

- Hydro-unit dynamics: Variations in water flow cause hydro turbines to behave nonlinearly, which has an impact on frequency regulation. It is difficult but essential to appropriately model these processes.
- Water level variations in reservoirs: these affect hydro production. Maintaining the stability of the system requires careful planning and cooperation.
- Interconnected grids: In a multi-area system, communication delays, inter-area oscillations, and sophisticated ALFC coordination can all have an impact on frequency regulation.
- Renewable integration: incorporating additional renewables (thermal, wind) impacts system dynamics and requires appropriate ALFC coordination.

- Governor and turbine control: the response time of the hydro governor influences ALFC, making it difficult to optimize control schemes.
- Frequency deviations: quick variations in load lead to frequency deviations; hence, efficient control mechanisms are required.

2.3.1 A Two-Area Interconnected Power System

Figure 2.4 depicts a two-area interconnected power system. These areas are linked via a tie line, enabling the bi-directional flow of electricity between them, while each area primarily serves its own local demand

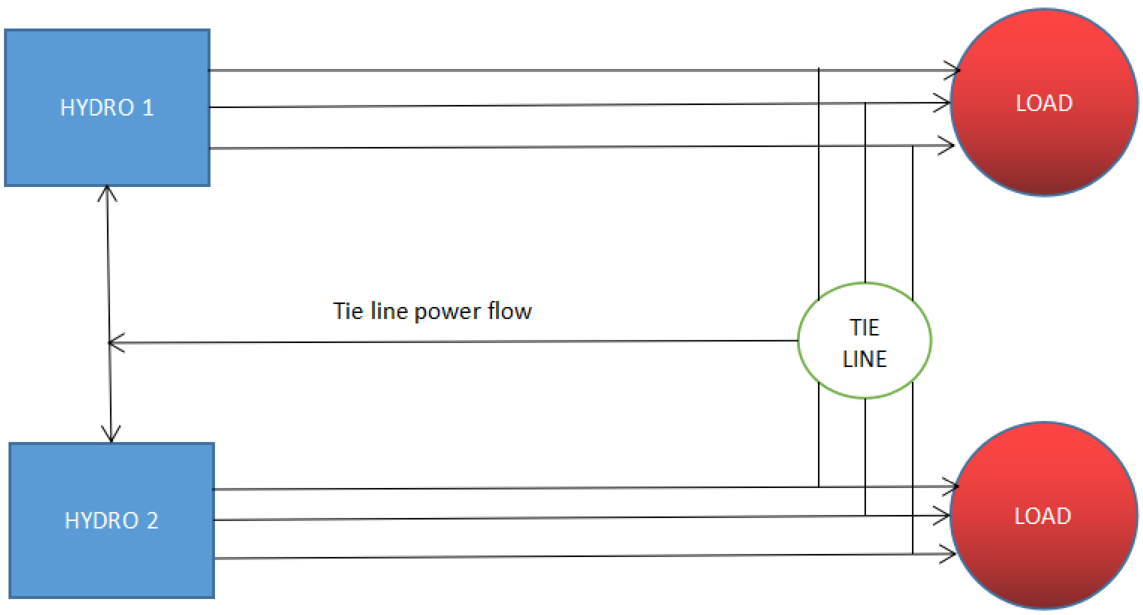

Figure 2.4 A two-area interconnected power system

An interconnected power system can be divided into control areas, each exhibiting strong internal coherence in frequency and voltage. These areas are linked by weaker tie-lines, allowing for power exchange while maintaining some independence. A system can have a single control area (the entire system acting as one) or multiple interconnected areas (Anower et al., 2016).

2.4 Conventional Vs 2DOF PID Controllers

In the hydropower system, the 2DOF PID controller has more advantages than conventional controllers like PI and PID regarding frequency set point tracking. During the starting of the turbine to load the generator the turbine speed must attain its nominal frequency (50 Hz). This action in hydro turbine is governed by two conventional controllers; PI and PID. PID controller is only used in isolated mode operation whereas PI controller is for parallel operation. So, due to this I preferred a PID-related good controller and selected the TDOF-PID controller. In this case, the controller should have a good ability to track the set point changes. During the normal operation, the set point is fixed to 50 Hz and the controller should have a good ability to regulate load disturbances. PI and PID controllers are limited in their ability to simultaneously track the set point and regulate load disturbances but a TDOF PID controller can overcome this limitation by introducing a second degree of freedom. This allows the controller to control both the set point and the disturbances independently, resulting in improved performance. So, using TDOF PID will solve such types of problems due to the following advantages.

- **Improved Set point Tracking and Disturbance Rejection:** TDOF PID controllers can achieve both fast set point tracking and disturbance rejection without compromising either performance objective. This is because they have an additional degree of freedom that allows them to independently adjust the response to set point changes and disturbances.
- **Reduced Overshoot:** TDOF PID controllers can significantly reduce overshoot, which is the transient response of the system exceeding the desired set point. This is particularly important for systems that require precise control and minimal overshoot, such as robotic manipulators and motion control systems.
- **Reduced Sensitivity to Load Variations:** TDOF PID controllers are less sensitive to load variations, which means they can maintain better control of the system even when the load on the system changes. This is important for applications where the load is unpredictable or constantly changing.
- **Enhanced Robustness:** TDOF PID controllers are more robust to plant model uncertainties, which means they can perform well even when the exact dynamics of the plant are not perfectly known. This is important in real-world applications where the plant model may be inaccurate or change over time.
- **Design Flexibility:** TDOF PID controllers provide more flexibility in design, allowing engineers to tailor the controller's behavior to specific application requirements. This includes the ability to adjust the relative weighting of the proportional, integral, and derivative terms.
- **Reduced Noise Sensitivity:** TDOF PID controllers can be more robust to noise in the input signal, which can lead to more stable and accurate control performance.

Overall, TDOF PID controllers offer several advantages over conventional PID controllers in terms of set-point tracking, overshoot, disturbance rejection, tuning flexibility, and robustness.

However, conventional are still widely used due to their simplicity and effectiveness in many applications.

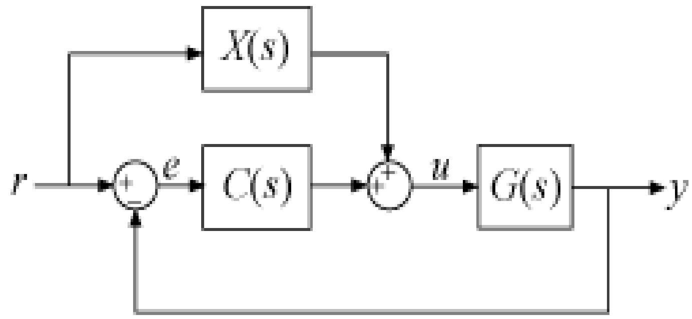

Figure 2.5 Two-degree-of-freedom (TDOF) control system (Deshmukh. & Kadu C.B., 2017)

Where r is the set-point variable, X(s) is the feed-forward compensator, C(s) is the serial compensator, e is the error, u is the controlled signal, G(s) is the plant and y is the output

$$C(s) = K_P + \frac{K_i}{s} + \frac{K_d s}{T_f s + 1} \tag{2.1}$$

$$X(s) = (b-1)K_p + \frac{(c-1)K_d s}{T_f s + 1} \tag{2.2}$$

Where K_P – is the proportional gain, K_i – integral gain, and K_d – derivative gain are the three parameters of C(s) which are known as the “basic parameters” whereas the two parameters of X(s) b and c are known as the “TDOF parameters”. T_f is derivative filter time.

2.5 Related Works

ALFC controllers play a crucial role in regulating power generation by processing incoming electrical demand requests and adjusting the ACE deviations. Traditionally, LFC design relied on classical control strategies, with controller parameters like pick-up values determined through a time-consuming trial-and-error approach. (Bevrani, 2009).

While trial-and-error approaches can determine controller settings, their performance suffers under varying system conditions. This has spurred research into more sophisticated controller design methodologies (Chaudhary Rahul & Singh Amar Preet, 2017). For the AGC of a networked hydropower plant, an intelligent controller was used. The conventional controller was evaluated with both FLC and ANN. The outcomes demonstrate that ANN and FLC perform better than PID controllers.

The authors (Annam Sirisha et al., 2017) investigated the performance of AGCs in interconnected power plants using various controllers, including fuzzy PI, PID, and PI. When contrasted with the PI controller, the AGC with the Fuzzy PI controller performed better.

In (Xiomara B. De La Cruz Molina, 2017) for large power plants, an optimal controller concept was used to boost the plant's efficiency. Because the feedback components of the ideal controller are entirely specified in terms of the function of the plant's state vector, the authors claimed that the realization of the controller was challenging and time-consuming.

The authors (Nagendra Kumar. et al., n.d.2019) Presents a model predictive control approach that was adopted in two and four thermal power plant areas. The MPC idea considers different load scenarios to assess how well the controllers perform compared to traditional PID controllers. According to the simulation results, the MPC scheme responds well in the short term and is resilient to load perturbations. Nevertheless, the study does not take into account the impact of communication delay connection, generation rate limitation, and governor deadband non-linearity.

(Fariya Tabassum. & M. S. Rana, n.d.2018) provide a comprehensive solution to address the issue of adjusting for frequency disturbances during load fluctuations. We are considering a two-area LFC power system with connectors. The dynamic response of the suggested controller is examined by contrasting it with existing AGC, PID, LQR, and fuzzy logic controllers. The simulation's output indicates that LQG performs better. Three regions of power systems operating under a deregulation scheme are described in the decentralized LFC problem (Mudi et al., 2019) A GA-based PID controller is presented in the study as a solution to the multi-area power system's decentralized LFC issue. In each control zone, the influence of the potential contracts is considered as a set of fresh input signals. The advantage of this technique is that it is not sensitive to significant load changes or disturbances when there are variations in plant parameters and nonlinearities in the system. With this method, the simulation's outcome indicates that the GA-based PID controller performs robustly.

The brilliant techniques based on intelligent techniques for illustration, The FLC based on the Fuzzy-PSO-PID with the application of UC and RFB was shown in(Joshi et al., 2023b). Regardless, a few investigators have observed a few confinements in GA, including meeting problems and traps in neighborhood minima, while attempting to determine the optimal solution to the problem. Because of its achievement proficiency and functional simplicity, the very well-proportional-integral operator is finest suited for secondary controller design. The dynamic properties of the impacted power generation are then improved by combining several TDOF-PID control systems (Arya, 2020).

In R. Shankar et al. (2017) This review comprehensively examines Automatic Generation Control strategies for conventional power systems, distributed generation, and microgrids, including the use of energy storage, FACTS devices, and HVDC links. However, it identifies a gap in exploring contemporary control methods like deep learning and reinforcement learning for optimizing AGC performance.

(Haes Alhelou et al., 2018) provided a comprehensive literature review on the different perspectives and challenges related to AGC in both traditional and future power systems. In this review, the authors first examined the use of AGC in diverse power system configurations and configurations. They then highlighted the applications of various intelligent and modern control methods for AGC.

(Veronica & Kumar, 2021) critically reviewed the different control strategies that have been employed for frequency regulation in standalone microgrids. This is a crucial issue, as microgrids often have a high penetration of renewable energy sources, which can introduce high levels of intermittency. The frequency regulation in autonomous microgrid operation is therefore a key challenge that requires effective control approaches.

(Barisal & Mishra, 2018) Investigates AGC for a two-area interconnected power system with unequal power distribution and diverse generation sources. It proposes using a PID controller tuned with three optimization algorithms: PSO, BFA, and an improved PSO variant incorporating "heavy search space compression" for faster convergence. The effectiveness of the optimized controller is evaluated by applying a 1% step load change in each area to assess the system's response. The authors (Haes Alhelou et al., 2019) The study investigated a decentralized AGC approach for a three-area power system with nonlinear considerations. This approach successfully maintained low interchange power and reduced frequency oscillations. However, the use of local observers in each area to approximate control signals raises concerns about system reliability in a decentralized structure. Since local controllers rely solely on their own data, potential inconsistencies can arise due to the simultaneous operation of these independent units. This highlights the limitations of traditional plant model-based AGC schemes in decentralized control systems (Xi et al., 2020) presented a thorough examination of the AGC regulator's multi-level control law application in a networked power system. Distributed controls are established at the coordination level, while centralized controls are enforced at the group level. the stability of the proposed control systems has been analyzed using the Lyapunov stability approach. This analysis has demonstrated that the control schemes exhibit greater stability, even at relatively large sample rates.

For the integration of significant amounts of wind power, the PO-TDOF-PID control technique-based AGC scheme is proposed by (Zhao et al., 2018) The regulation strategy has been designed to minimize variability and enhance the system's inertial response. This regulation approach has been evaluated for three-area power systems, considering both high and low wind power production scenarios in each case. The analysis has shown that the proposed control solution provides a satisfactory way to mitigate the adverse effects introduced by the integration of wind power into the AGC system.

Inference:

The literature review highlights that traditional frequency regulation approaches based on classical PID controllers have limitations in dealing with varying system conditions and disturbances. This has led researchers to explore more advanced control methodologies, including intelligent techniques like fuzzy logic control, artificial neural networks, and model predictive control. Several studies have demonstrated the superior performance of these advanced controllers compared to conventional PID designs for automatic generation control (AGC) in interconnected power systems. However, there is still a need to optimize the control parameters further and address challenges like communication delays, generation rate limitations, and governor deadband nonlinearities. Here, most researchers have used unoptimized TDOF PID.

This thesis work on the design of a PSO-based two-degree-of-freedom PID controller for two-area hydropower plants aims to address some of these gaps by leveraging the benefits of intelligent optimization techniques and flexible control structures.

CHAPTER THREE

MATERIALS AND METHODS

3.1 Materials used

3.1.1 Hardware and software used:

- Computer
- MATLAB software R2021a for simulation purposes
- Math type 7.0
- Mendeley desktop
- Microsoft Office 2016

3.1.2 Sites chosen and data collected:

- Koka (Awash I) hydroelectric power station.

  Koka hydroelectric power plant Construction started in 1957 and formally concluded in 1960. The station is located in the Oromia region approximately 80km east of Addis Ababa. Besides power generation, it is also used for floodwater regulation and the fishing industry. It was the first big electric-producing power station in Ethiopia. The Koka Dam is a concrete gravity dam, with a crest length of 430 meters and a maximum height of 47 meters, Its reservoir has a total storage capacity of 1.3 billion cubic meters. The surface powerhouse facility is situated on the left bank of the river and has three Francis turbine units. Each of these turbine generators has a nominal power output rating of 14.4 megawatts.

  It also has a penstock all 3.5 m in diameter. Each penstock is connected to each turbine. The switchyard is installed with three step-up transformers of 18MVA to convert the voltage from 10.5kV to 132kV. It includes a double bus-bar scheme, linking seven three-phase 132kV transmission lines. The total potential electric output is 110 GWH/year

- Awash II and III hydroelectric power station.

  Awash II and III hydroelectric power plants were Constructed in 1966 and formally concluded in 1971. The station is located in the Oromia region approximately 104km east of Addis Ababa. Besides power generation, it is also used for irrigation. Its water management depends on Koka HEPP and it is a run-off type power generation station. Contains four Francis turbines each with a nominal power output of 16 MW.

It also includes a penstock 3 m in diameter. Each tunnel is connected to each turbine. The switchyard is installed with four step-up transformers of 18MVA to convert the voltage from 10.5kV to 132kV. It includes a double bus-bar scheme, linking six three-phase 132kV transmission lines. The total potential electric output is 182 GWH/year

Koka and Awash II HEPP governor, turbine, and generator electrical drawing with parameter settings.

Ethiopia load dispute center (LDC) energy data for different three months.

Validation of blackouts in Ethiopia from Koka HEPP.

Table 3.1 Hydropower stations description.

Descriptions	Koka (Awash I)	Awash II AND III
Generation capacity (MW)	43	64
Generator type	Synchronous	Synchronous
Generator MVA(MVA)	18	20
Operating Load (MW)	43	60
Type of turbine	Francis	Francis
Capacity factor	0.23	0.21
Bus transmission voltage (KV)	132	132

Figure 3.1 Location of the power plants on a map.

3.2 Methods

To complete the required works for this thesis, some procedures have been followed as shown in Figure 3.2. Literature related to this topic has been studied, and important data are collected and analyzed. Then mathematical and graphical analysis of collected data informs the development of a system model

In system modeling the mathematical model for one area and two-area hydropower system is modeled and the simulations are implemented on MATLAB/Simulink and simulation results are analyzed and compared with other related techniques.

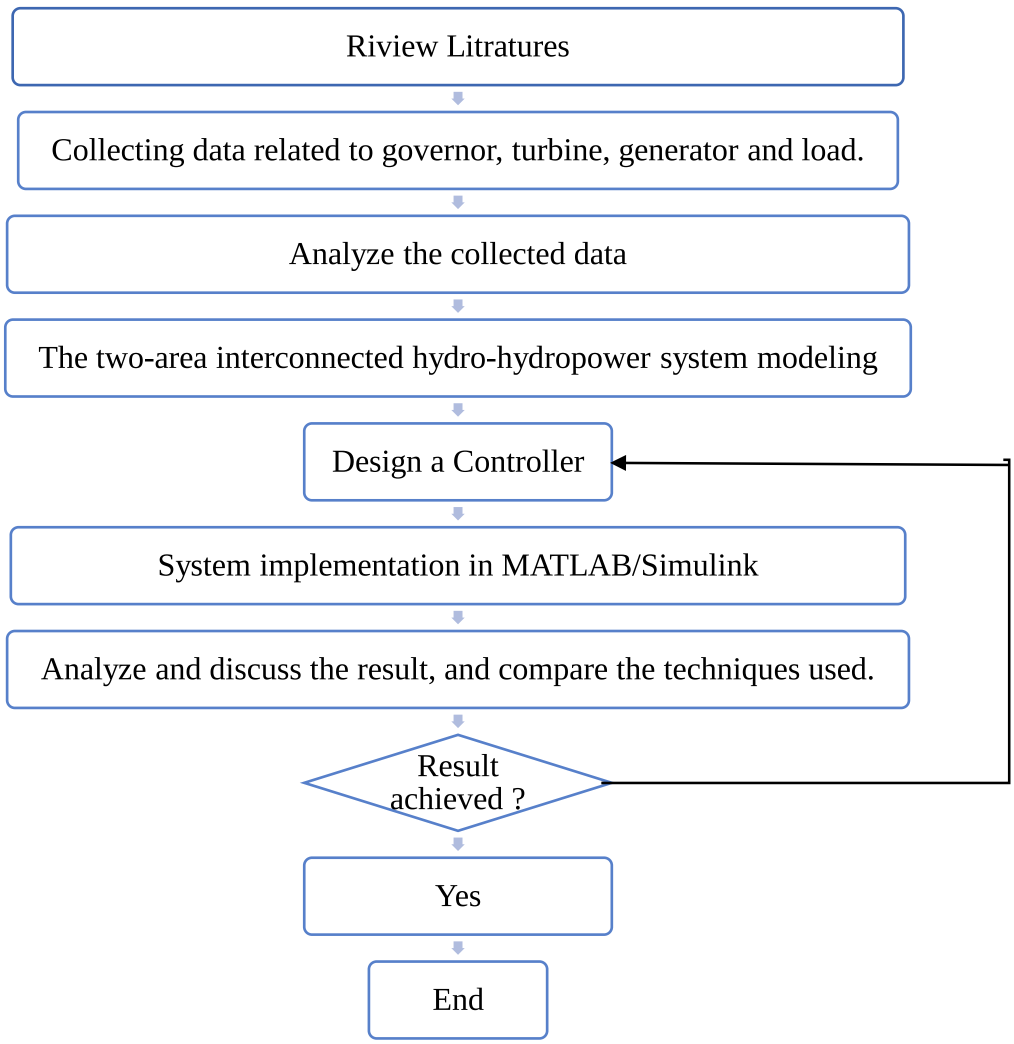

Figure 3.2 Block diagram representation of the work flow of the thesis

3.3 Modelling Hydro-power plan

Modeling hydro-power plants for improving hydro unit dynamics involves optimizing the control mechanisms and understanding the underlying dynamics. Here are some strategies

- Water flow control- implement effective water flow control strategies. This includes managing reservoir level, gate opening, and spillways to maintain stability.
- Inertia enhancement- consider adding flywheels or other energy storage systems to enhance system inertia. This helps stabilize frequency during disturbances
- Speed regulation- Enhancing speed regulation by minimizing mechanical losses and ensuring efficient energy conversion for proper maintenance of the turbine and generator is crucial.
- Frequency response- design control schemes that respond quickly to frequency deviations
- Tuning- properly tuning the hydro-governor and controller parameters to achieve the desired response time.
- Modeling and simulation- develop an accurate mathematical model for the hydro turbine and governor considering water flow variation and other relevant factors.

All Generators in the power system have a response to the changes in frequency via their turbine speed governor which is used in regulating the input of the wicket gates of the turbine. When the load varies the water entering into the turbine varies proportionally which is governed by the opening of the wicket gates through the turbine speed governor by affects the turbine speed. When a load increases in a certain control area it is firstly provided by the kinetic energy stored in the rotating mass of the turbine which results in a drop in the system frequency throughout the interconnected power system.

During the change in speed or frequency, all the generators must adjust their frequency to the new steady state value by creating a balance between the system load and the generator power. It is the main duty of the ALFC in the disturbed control area to adjust its generation in anytie-line interchange. The power variation that resulted from the load change is returned to null, and the new steady state frequency is brought back to its nominal value.

For an isolated power system, the ALFC is responsible for maintaining the nominal frequency related to its load only. For a large power system, regulating the frequency is a challenging task so, understanding the characteristics of the power system equipment is a major task in studying ALFC. The figure below describes the basic control structure of the electric power system.

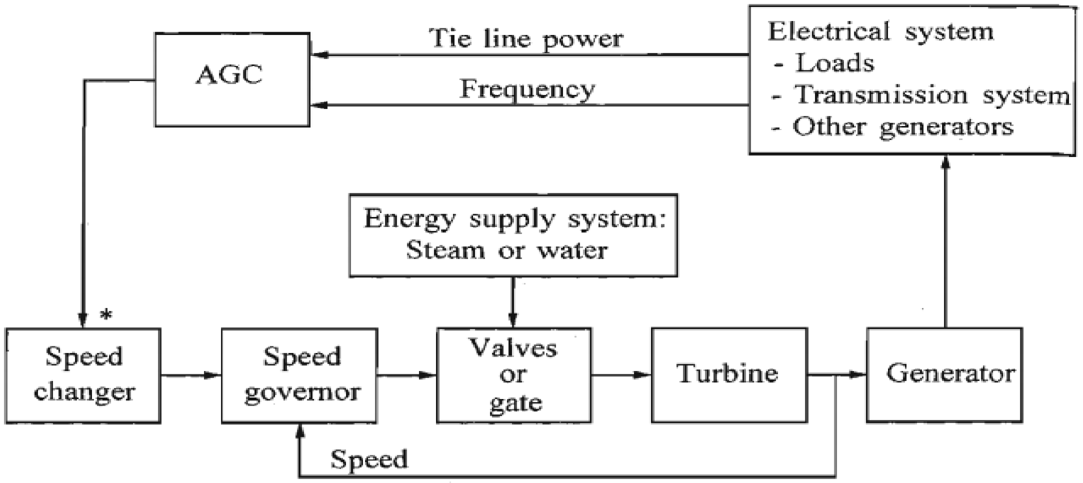

Figure 3.3 Functional block diagram of power generation and control system (Kundur & Malik, n.d.-a)

The ALFC detects the change in the tie-line power and frequency and gives the order to the unit controller to adjust the gates for water in late to the turbine via the speed governor. When the turbine adjusts its rotating speed, the generator responds to the change in frequency as well as the tie-line power. These problems with ALFC exist since operating conditions are continually changing.

3.3.1 Turbine Speed Governor Model

The speed governor is one of the basic units in power generation that senses the frequency variation and keeps the generator power constant. Governor output operates all the time on wicket gate servomotors to determine the right water flow through the turbine governor also operates wicket gates differently at turbine start and stop(*Operation and Maintenance Manual DWG. NO. 2*, n.d.). The main governor functional units are turbine speed measurement, controller, power control loop, speed drop, opening limiter, positioning loop for wicket gates servomotors, and logic units for governor starting and stopping operations.

In parallel operation, system frequency dictates generator speed. While the governor's reference signal remains constant, frequency deviations trigger power adjustments based on the droop settings, reflecting its active role in primary frequency regulation. However, operating the wicket gates controlled by the governor requires considering the interposed servo motor's dynamics.

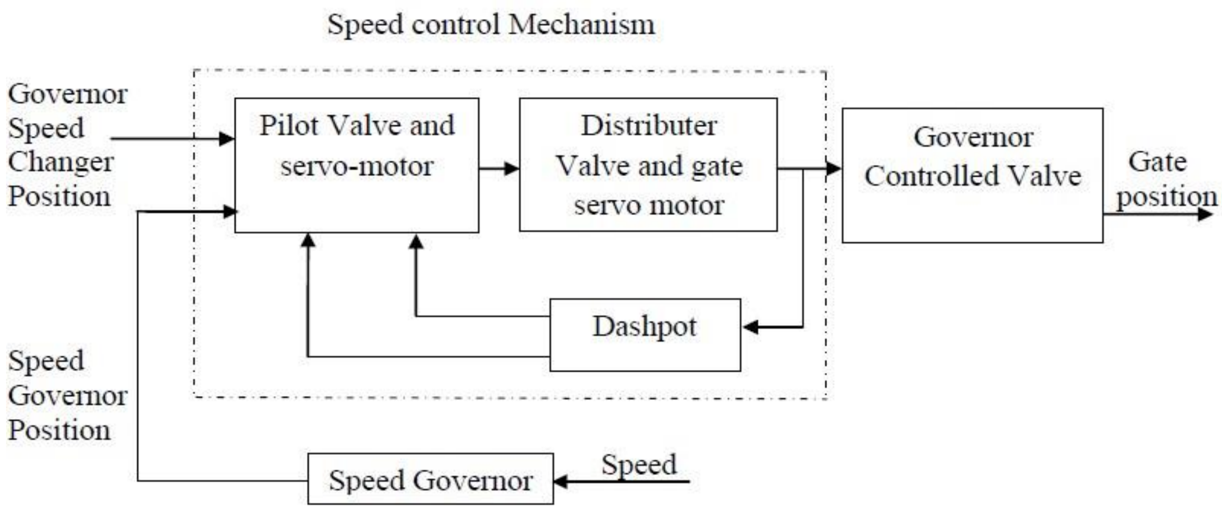

Figure 3.4 Block diagram of a hydro governor (Leul, 2018)

In this governor system, servo motors provide the necessary torque to adjust wicket gates, while the dashpot acts as a deviation feedback mechanism to maintain the permanent droop (R_p) by counteracting any deviations from the desired position The transfer function of the dashpot is given as:

$$\frac{R_T s T_R}{1+sT_R} \tag{3.1}$$

Where R_T is called the tangent droop.

The other feedback is through permanent droop to determine the net droop. The transfer function of the water turbine speed governor with various blocks is shown below.

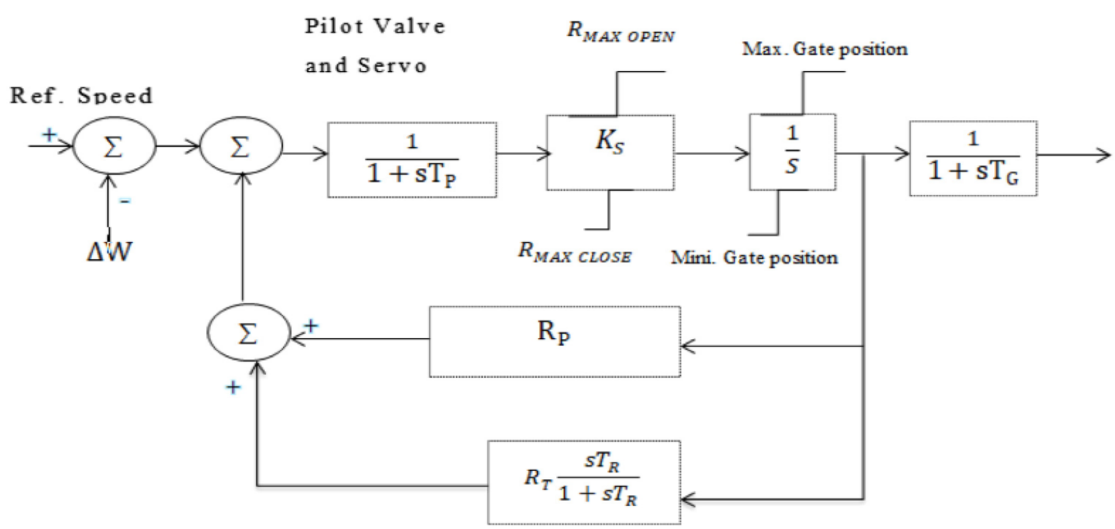

Figure 3.5 Block diagram of the electronic governor (Weldcherkos et al., 2021)

The secondary loop in the system is very useful regarding the response for water flow harnessing, thus considering the water level of the reservoir it allows sustainable and quality power generation.

Where Constraints: Maximum gate position limit = 1.0

Minimum gate position limit = 0

$R_{max-open}$ = maximum gate opening rate = 0.16 p.u/s

$R_{max-close}$ = maximum gate closing rate= 0.16 p.u/s

$R_{max-buff}$ = maximum gate closing rate in buffered region = 0.04 p.u/s

G_{buff} = buffered region in p.u. of servomotor stroke = 0.08 p.u.

Whereas S_R is the reference speed, ΔW speed deviation

The time constant T_R depends on the motor starting time constant (T_m) which is given by:

$$T_R = 5T_m \tag{3.2}$$

$$R_T = \frac{2.5T_m}{H} \tag{3.3}$$

Where H is the inertia of the turbine.

Then the general transfer function of the speed governor can be modelled as below:

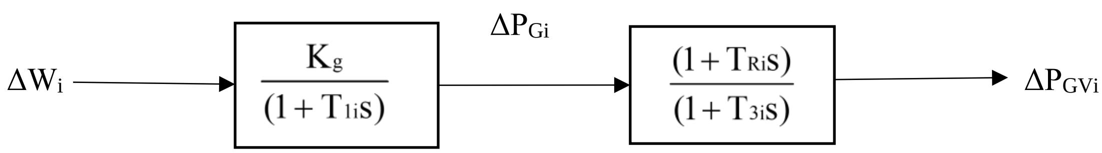

Figure 3.6 Block diagram of speed governor

Where ΔW_i – speed deviation, ΔP_{Gi}– change in governor servomotor position, Kg– Governor Gain, T_{1i}-speed governor rest time, ΔP_{GVi} – gate valve position deviation, T_{Ri} - Transient droop time constant and T_{3i} - main servo time constant

Figure 3.7 Governor of Koka and Awash II HEPP

3.3.2 Turbine Modelling

In this section, the physical description of the penstock-hydraulic turbine and characteristic equations that are suitable for mathematical models of their representation in power system dynamics are presented (Allen J Wood et al., n.d.). Here we have to consider a penstock turbine having an effective length of L discharging water to the turbine at a velocity of V feet per second operating at a head of H.

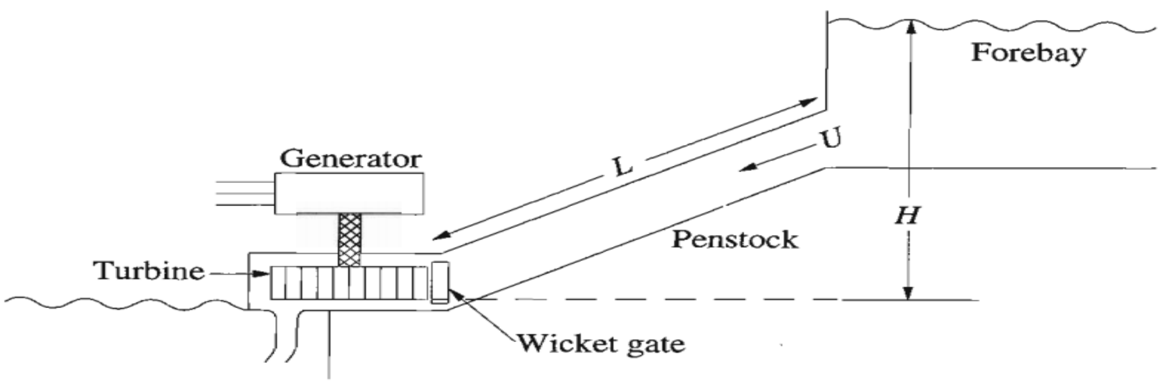

Figure 3.8 Schematic of a hydroelectric plant (Kundur & Malik, n.d.-a)

As water flows from the storage tank through the penstock, its dynamics influence the hydro turbine's transient behavior. By analyzing these dynamics and linearizing the governing equations around a steady state, we can derive the transfer function of the hydro turbine:

$$q = a_{11}h + a_{12}v + a_{13}g \quad (3.4)$$

$$t = a_{21}h + a_{22}v + a_{23}g$$

where q- deviation inflow in per unit, h - change in the head in per unit, v - change in speed in per unit, g- variation in gate position in per unit, and t - variation in torque in per unit.

The provided algebraic equations in equation (3.4) relate changes in water flow to variations in head and gate position, similar to how a change in torque relates to small variations in head, speed, and gate position in a hydro-turbine. By leveraging these equations along with the penstock's water flow dynamics, a transfer function model can be derived to express the hydro-turbine's mechanical power output as a function of gate position.

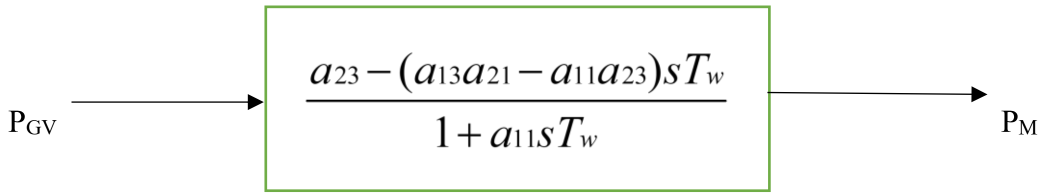

Figure 3.9 Block diagram of turbine model

Where P_{GV} – position of gate, P_M - mechanical time constant, T_W - water Time constant

The coefficient in the two algebraic equations can be interpreted as prior derivatives of deviation in flow (q) concerning head, speed, and gate position. Similarly, derivatives of torque (t) concerning head, speed, and gate position as described below:

$$a_{11}=\frac{dq}{dh},\ a_{12}=\frac{dq}{dv},\ a_{13}=\frac{dq}{dg}, \tag{3.5}$$

$$a_{21}=\frac{dt}{dh},\ a_{22}=\frac{dt}{dv},\ a_{23}=\frac{dt}{dg}$$

For the design purpose, a lossless ideal turbine at nominal speed and head are considered with the following parameters. Where a_{11}= 0.5, a_{12}= 0, a_{13}= 1, a_{21}= 1.5, a_{22}= -1, and a_{23}= 1

If we make use of these values and substitute them in the above block diagram it can be reduced to the block diagram shown below:

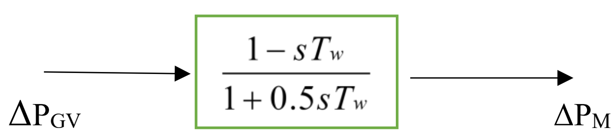

Figure 3.10 Reduced block diagram of hydro turbine

Figure 3.11 Turbine and servo system of Koka and Awash II HEPP

3.3.3 Synchronous Generator-Load Model

In electrical power systems, synchronous generators, the workhorses of electricity generation, maintain consistent electrical frequency by matching their electrical power output (torque) to the system load. Any change in load instantly disrupts this balance between the generator's electrical torque and the mechanical torque from its rotation (Fardo & Patrick, n.d.). This is designated as a net accelerating or decelerating torque.

$$T_a = T_m - T_e \tag{3.6}$$

Where T_a -is a net accelerating torque (N.m), Tm - is a machine mechanical torque (N.m) and Te is an electrical torque (N.m).

In generators, the positive imbalance between electrical and mechanical torques causes the combined inertia of the generator and prime mover to accelerate. This gives us the equation of motion labelled as:

$$J\frac{dW_m}{dt} = T_a = T_m - T_e \tag{3.7}$$

where J – is the generator combined moment of inertia in the turbine ($Kg.m^2$), W_m- is the rotor angular velocity (mech. rad/sec), T-time (sec).

Defining the inertia constant H as the kinetic energy in watt-seconds divided by the VA base as shown below.

$$H = \frac{1}{2}\frac{J_{W_{MO}}{}^2}{VA_{base}} \tag{3.8}$$

Then, J- can be written in terms of H as:

$$J = \frac{2H}{w_{0m}{}^2}VA_{base} \tag{3.9}$$

Substituting equation (3.9) in equation (3.7)

$$\frac{2H}{W_{Om}{}^2}VA_{base}\frac{dW_m}{dt} = T_m - T_e \tag{3.10}$$

The per-unit form of equation (3.8) is:

$$T_{base} = \frac{VA_{base}}{W_m} \tag{3.11}$$

$$2H\frac{d\overline{\mathrm{W}_r}}{dt} = \overline{T_m} - \overline{T_e} \tag{3.12}$$

$$\overline{W_r} = \frac{W_m}{W_{mo}} = \frac{W_r}{W_o} \tag{3.13}$$

Where Wr is the angular velocity of the rotor [rad/s], and at rated speed, W_0 is the rated angular velocity [rad/s].

Here $\overline{Wr}, \overline{T}_{m,} T_e$ per-unit quantities of W_r, $T_{m,}$ and T_e respectively. The mechanical starting time setting is described as:

$$M = 2H(s) \tag{3.14}$$

The equation of motion can be written as:

$$M\frac{d\overline{Wr}}{dt} = \overline{T}_m - \overline{T}_e \tag{3.15}$$

Within this study of Automatic Load Frequency Control (ALFC), we'll use 'M' and 'H' interchangeably to denote the inertia constant. However, for clarity, Eq. (3.15) will be expressed in terms of mechanical and electrical power instead of torque. The relationship between power P and torque T *is* given by:

$$P = W_r T \tag{3.16}$$

Since we are considering small change (denoted by the prefixΔ) from initial values (denoted by subscript), we may write;

$$\begin{aligned} P &= P_0 + \Delta P \\ T &= T_0 + \Delta T \\ W_r &= W_0 + \Delta W_r \end{aligned} \tag{3.17}$$

Substituting equation (1.17) in equation (1.16) we have:

$$P_0 + \Delta P = (W_0 + \Delta W_r)(T_0 + \Delta T) \tag{3.18}$$

Ignoring higher-order terms and considering only the relationship between changed values give us:

$$\Delta P = W_0 \Delta T + \Delta W_r \Delta T \tag{3.19}$$

Hence;

$$\Delta P_m - \Delta P_e = W_0(\Delta T_m - \Delta T_e) + \Delta W_r(T_{m0} - T_{e0}) \tag{3.20}$$

In steady state conditions, the mechanical torque and electrical torque are equal, and the speed expression in per unit w_0=1; equation (3.20) can be:

$$\Delta P_m - \Delta P_e = \Delta T_m - \Delta T_e \tag{3.21}$$

Therefore, the equation of the motion can be rewritten as:

$$M\frac{dW_r}{dt} = P_m - P_e \tag{3.22}$$

Where M is expressed in seconds and others are in per unit. For analysis of power system dynamics performance, the above motion equation can be represented in the Laplace domain as:

$$Ms\Delta W_r = \Delta T_m - \Delta T_e \tag{3.23}$$

Solving for change in frequency can be expressed as:

$$\Delta W_r = \frac{1}{Ms}(\Delta T_m - \Delta T_e) \tag{3.24}$$

Following this, the expression for the change in electrical power considers both resistive (independent of frequency) and motor (frequency-dependent) load components is:

$$\Delta P_e = \Delta P_L + D\Delta W_r \tag{3.25}$$

Where ΔP_e is the non-frequency sensitive load change, $D\Delta W_r$ is the frequency-sensitive load change, and D is the load-damping constant.

The damping constant is represented as a one percent change in frequency caused by a one percent change in load. Substituting Equation (3.25) into Equation (3.24) and solving for the frequency change gives:

$$\Delta W_r = \frac{1}{Ms + D}(\Delta T_m - \Delta T_L) \tag{3.26}$$

This equation captures the dynamic behavior of the synchronous generator, relating frequency deviations to the imbalance between power generation and load demand. It incorporates the system's total inertia and accounts for both frequency-dependent and independent load components. The equation is particularly relevant for power systems with multiple generating units, it can be described as:

$$\Delta W_r = \frac{1}{M_{eq}s + D}(\Delta T_{mi} - \Delta T_L) \tag{3.27}$$

$$M_{eq} = \sum M_i(s) \tag{3.28}$$

Where ΔT_{mi} is the change in mechanical power of the i^{th} generating unit, $M_i(s)$ is the inertia constant of the i^{th} generating unit.

Assuming al1 generators respond consistently to changes in system load enabling them to be represented by an equivalent generator model block diagram representation as shown below.

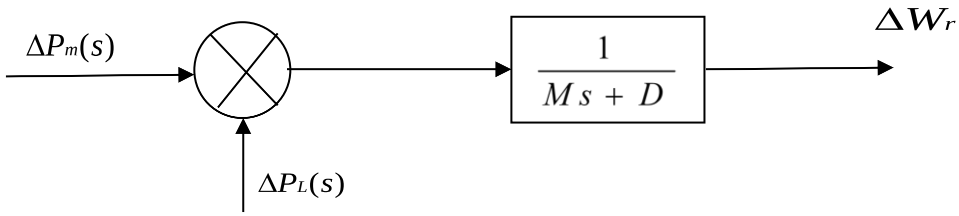

Figure 3.12 Block diagram of synchronous generator

3.4 Tie Line Modelling

In interconnected power systems, tie-line bias control, a strategy used in Automatic Generation Control, leverages the simplicity and reliability of tie-lines to maintain system frequency. This approach allows each area to independently manage generation and fulfill its control obligations (ACE) by monitoring the frequency difference and resulting power exchange across the tie-line. The tie-line power (Tab) in a two-area system is determined by both the scheduled power exchange (Pab) between areas A and B and the inherent synchronization torque coefficient of the tie-line itself. This implies that the integral of the frequency difference between the two areas reflects the power imbalance caused by tie-line mismatches

Figure 3.13 Block diagram of Tie line Power transfer

In Figure 3.13, there are two control areas, and the tie line power transferred between them is denoted by P_{tie12}, the reactance between those areas is denoted by X12, and the magnitude of the voltage in area 1 and area 2 is denoted by |V1| and |V2| respectively.

$$P_{tie12} = \frac{|V_1||V_2|}{X_{12}} \sin(\theta_1 - \theta_2) \tag{3.29}$$

The subscripts (1 and 2) indicate a positive power flow from bus 1 to bus 2 on the tie line. For small angle deviations (ΔΘ1 and ΔΘ2), the change in tie-line power (ΔPtie) is described by the following equations (3.30), and (3.31):

$$\Delta P_{tie12}(pu) = \frac{|V_1||V_2|}{X_{12}} \cos(\theta_1 - \theta_2)(\Delta\theta_1 - \Delta\theta_2) \tag{3.30}$$

$$\Delta P_{tie12}(pu) = T_{12}(\Delta\theta_1 - \Delta\theta_2) \tag{3.31}$$

Where $T_{12} = \frac{|V_1||V_2|}{P_{r1}X_{12}}\cos(\theta_1 - \theta_2)$ - synchronizing constant (3.32)

Equation (3.30) can be rewritten as:

$$\Delta P_{tie12} = 2\pi T_{12}\left(\int \Delta f_1 dt - \int \Delta f_2 dt\right) \tag{3.33}$$

Where Δf_1 and Δf_2 are frequency deviations in area-1 and area-2 respectively.

Similarly, power flowing from area-2 to area-1 can be given as:

$$\Delta P_{tie21} = 2\pi T_{21}\left(\int \Delta f_2 dt - \int \Delta f_1 dt\right) \tag{3.34}$$

$$T_{21} = \frac{|V_2||V_1|}{P_{r2}X_{21}}\cos(\theta_2 - \theta_1) \tag{3.35}$$

Where P_{r1} and P_{r2} are the rated capacity of area-1 and area-2 respectively.

From equation (3.33) and (3.34) we get:

$$\Delta P_{tie21} = a_{12}\Delta P_{tie12} \tag{3.36}$$

Where: $a_{12} = \frac{P_{r1}}{P_{r2}}$

About eqn. (3.25) incremental power balance equation for area-1 can be written as:

$$\Delta P_{e1} - \Delta P_{L1} = \frac{2H}{f_0}\frac{d(\Delta f_1)}{dt} + D_1\Delta f_1 + \Delta P_{tie12} \tag{3.37}$$

Taking Laplace transform and arranging we have:

$$\Delta f_1 = [\Delta P_{e1}(s) - \Delta P_{L1}(s) - \Delta P_{tie12}(s)]\frac{K_{p1}}{(1 + sT_{p1})} \tag{3.38}$$

Where: $K_{p1} = \frac{1}{D_1}; T_{p1} = \frac{2H_1}{D_1 f_0}$

Hence; the block diagram representation of eqn. (3.38) is given as in Figure 3.14 below.

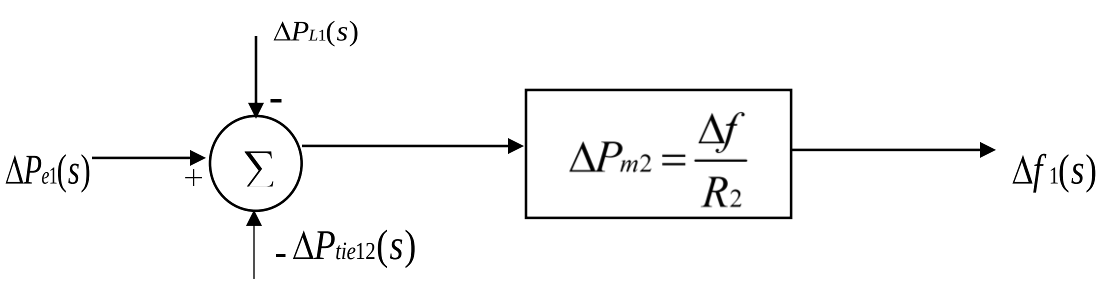

Figure 3.14 Area one generator and load block diagram

Similarly, for area 2 the block diagram representation is given in the figure below.

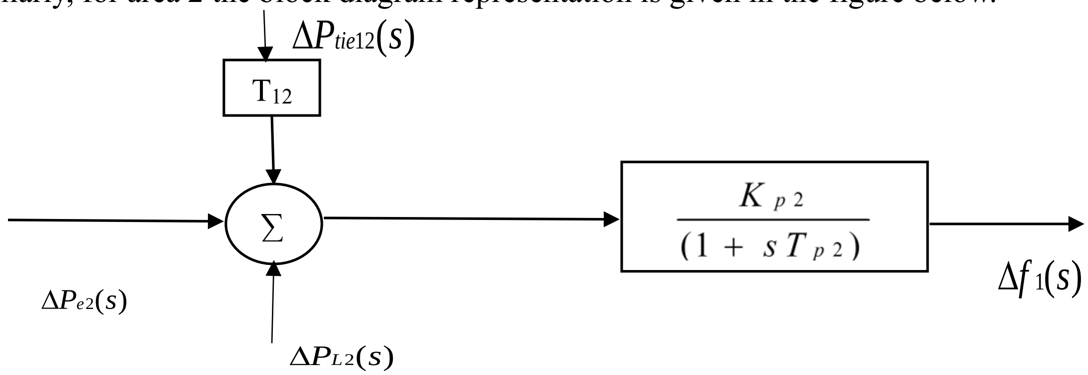

Figure 3.15 Area two generator and load block diagram

Taking the Laplace of equation (3.33), we get:

$$\Delta P_{tie12}(s) = \frac{2\pi T_{12}}{s}[\Delta f_1(s) - \Delta f_2(s)] \tag{3.39}$$

Then the block diagram representation of the tie line power is represented in Figure (21).

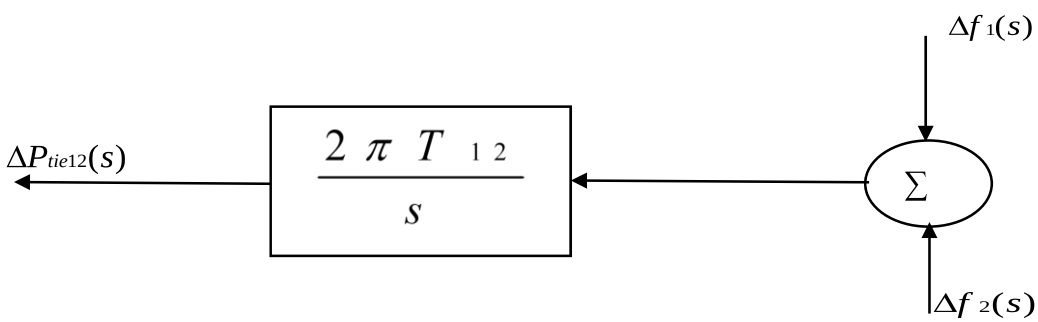

Figure 3.16 Block diagram representation of tie-line power

With each system area represented by an equivalent inertia M, load damping constant D, turbine, and governing system with an effective speed droop R; the tie-line is represented by the synchronizing torque coefficient T_{12} a positive ΔP_{tie12} represents an increase in power transfer from area-1 to area-2. This effect is equivalent to increasing the load of Area 1 and decreasing the load of Area 2; therefore, feedback ΔP_{tie12} has a negative sign for Area 1 and a positive sign for Area 2.

The steady-state frequency deviation is the same for the two areas. For a total load change of ΔP_L.

$$\Delta f = \Delta W_1 = \Delta W_2 = \frac{-\Delta P_L}{(\frac{1}{R_1} + \frac{1}{R_2}) + (D_1 + D_2)} \tag{3.40}$$

Considering the steady-state values following an increase in area-1 load by $\Delta P_{L.}$

for area-1, we have:

$$\Delta P_{m1} - \Delta P_{tie12} - \Delta P_{L1} = \Delta f D_1 \quad (3.41)$$

For area-2;

$$\Delta f\,(\frac{1}{R_2} + D_2) = \Delta P_{tie12} \quad (3.42)$$

The change in mechanical power depends on regulation.

Hence,

$$\Delta P_{m1} = \frac{\Delta f}{R_1} \quad (3.43)$$

$$\Delta P_{m2} = \frac{\Delta f}{R_2} \quad (3.44)$$

Substituting equation (3,43) in equation (3.41) and equation (3.44) in equation (3.42) gives

$$\Delta f\,(\frac{1}{R_1} + D_1) = -\Delta P_{tie12} - \Delta P_L \quad (3.45)$$

And $\Delta f\,(\frac{1}{R_2} + D_2) = \Delta P_{tie12}$ (3.46)

Solving equation (3.45) and (3.46), we get:

$$\Delta f = \frac{-\Delta P_L}{(\frac{1}{R_1} + D_1) + (\frac{1}{R_2} + D_2)} = \frac{-\Delta P_L}{\beta_1 + \beta_2} \quad (3.47)$$

And $\Delta P_{tie12} = \dfrac{-\Delta P_L(\frac{1}{R_2} + D_2)}{(\frac{1}{R_1} + D_1) + (\frac{1}{R_2} + D_2)} = \dfrac{-\Delta P_L \beta_2}{\beta_1 + \beta_2}$ (3.48)

Where β_1 and β_2 are the frequency bias or the frequency response characteristics of area-1 and area-2 respectively.

3.5 Two-area Power System Modelling

In an interconnected power system, which is linked by a tie-line; the tie-line is essential in controlling the frequency and power flow deviation. Since the goal of LFC is not only to cancel frequency error, it also drives the tie-line power exchange based on the demand by driving the ACE in all areas to zero. For both power generation areas, this ACE is used as the plant output. When we set the ACE to zero, the frequency error and the tie-line power error will be zero. So by interconnecting areas with power-producing units, we can attain the best frequency and tie-line power. Hence, we need to include the information of the tie-line power deviation into our control input the ACE can be well-defined as:

$$ACE_a = \sum_{b=2,\ldots n} \Delta Pt_{ieab} + \beta_a \Delta f_a \tag{3.49}$$

$$\beta_a = D_a + \frac{1}{R_a} \tag{3.50}$$

Where β_a is frequency bias for area-a

For two interconnected areas, the ACE is calculated as:

$$\begin{aligned} ACE_1 &= \Delta Pt_{ie12} + \beta_1 \Delta f_1 \\ ACE_2 &= \Delta Pt_{ie21} + \beta_2 \Delta f_2 \end{aligned} \tag{3.51}$$

While the makeup of Area Control Error (ACE) signals is crucial, this work prioritizes their impact on the transient response of the Load Frequency Control (LFC) system, particularly in response to a sudden load increase in Area 1. As demonstrated by equation (3.47), a sudden load increase will lead to a reduced frequency excursion, ultimately bringing the frequency deviation back within acceptable limits due to the regulating characteristics of both interconnected areas.

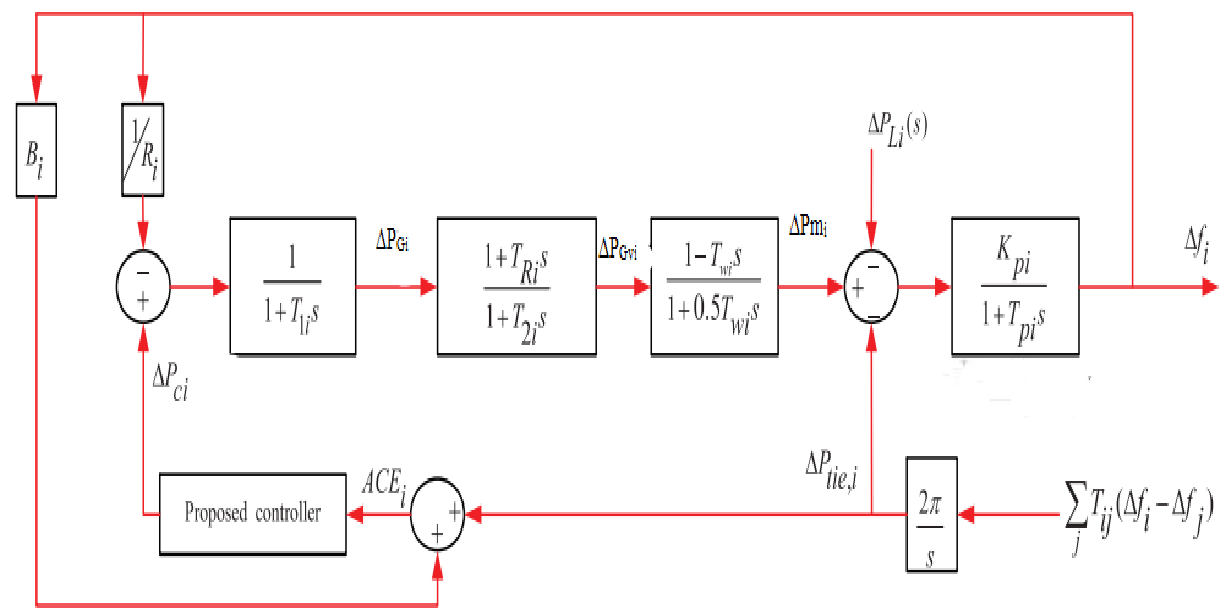

Figure 3.17 Block diagram of the hydro-power plant with change in tie-line power (i=1,2)(AH & Li, 2020)

In this block diagram, for each control area, there are three inputs (the controller input U, load disturbance ΔP_L, and tie-line power error $\Delta P_{12)}$ and two outputs (one ACE output, and one generator output Δf).

The overall generator-load dynamics relationship between the incremental mismatch power and the frequency deviation can be expressed as:

$$\Delta\dot{f}_i = -\frac{1}{T_{Pi}}\Delta f_i - \frac{K_{Pi}}{T_{Pi}}\Delta P_{tie,i} + \frac{K_{Pi}}{T_{Pi}}\Delta P_{Gi} - \frac{K_{Pi}}{T_{Pi}}\Delta P_{Li} \tag{3.52}$$

The model of the speed governing system is modeled as:

$$\Delta\dot{P}_{GVi} = -\frac{T_{2i}}{T_{1i}T_{3i}R_i}\Delta f_i - \frac{1}{T_{3i}}\Delta P_{GVi} + \left(\frac{1}{T_{3i}} - \frac{T_{2i}}{T_{1i}T_{3i}}\right)\Delta P_{Gi} + \frac{T_{2i}}{T_{1i}T_{3i}}\Delta P_{ci} \tag{3.53}$$

$$\Delta\dot{P}_{Gi} = -\frac{1}{T_{1i}R_i}\Delta f_i - \frac{1}{T_{1i}}\Delta P_{Gi} + \frac{1}{T_{1i}}\Delta P_{ci} \tag{3.54}$$

The model of the turbine and water dynamics can be calculated as:

$$\Delta\dot{P}_{mi} = -\frac{2T_{2i}}{T_{1i}T_{3i}R_i}\Delta f_i - \frac{2}{T_{wi}}\Delta P_{mi} + \left(\frac{2}{T_{wi}} + \frac{2}{T_{3i}}\right)\Delta P_{GVi} - \left(\frac{2}{T_{3i}} - \frac{2T_{2i}}{T_{1i}T_{3i}}\right)\Delta P_{Gi} - \frac{2T_{2i}}{T_{1i}T_{3i}}\Delta P_{ci} \tag{3.55}$$

The tie-line power between area-i and area-j can be formulated as:

$$\Delta\dot{P}_{tie,ij} = 2\pi T_{ij}(\Delta f_i - \Delta f_j);\ \Delta P_{tie,ij} = \Delta P_{tie,ji} \tag{3.56}$$

Based on the above analyses the state model is given as:

$$\begin{bmatrix} \Delta\dot{f}_i \\ \Delta\dot{P}_{tie,i} \\ \Delta\dot{P}_{mi} \\ \Delta\dot{P}_{Gi} \\ \Delta\dot{P}_{GVi} \end{bmatrix} = \begin{bmatrix} -\frac{1}{T_{Pi}} & -\frac{K_{Pi}}{T_{Pi}} & \frac{K_{Pi}}{T_{Pi}} & 0 & 0 \\ 2\pi T_{ij} & 0 & 0 & 0 & 0 \\ -\frac{2T_{2i}}{T_{1i}T_{3i}R_i} & 0 & -\frac{2}{T_{wi}} & \left(\frac{2T_{2i}}{T_{1i}T_{3i}} - \frac{2}{T_{3i}}\right) & \left(\frac{2}{T_{wi}} + \frac{2}{T_{3i}}\right) \\ -\frac{1}{T_{1i}R_i} & 0 & 0 & -\frac{1}{T_{1i}} & 0 \\ -\frac{T_{2i}}{T_{1i}T_{3i}R_i} & 0 & 0 & \left(\frac{1}{T_{3i}} - \frac{T_{2i}}{T_{1i}T_{3i}}\right) & -\frac{1}{T_{3i}} \end{bmatrix} \begin{bmatrix} \Delta f_i \\ \Delta P_{tie,i} \\ \Delta P_{mi} \\ \Delta P_{Gi} \\ \Delta P_{GVi} \end{bmatrix} +$$

$$\begin{bmatrix} 0 \\ 0 \\ -\frac{2T_{2i}}{T_{1i}T_{3i}} \\ \frac{1}{T_{1i}} \\ \frac{T_{2i}}{T_{1i}T_{3i}} \end{bmatrix} \Delta P_{ci} + \begin{bmatrix} -\frac{K_{Pi}}{T_{Pi}} \\ 0 \\ 0 \\ 0 \\ 0 \end{bmatrix} \Delta P_{Li}$$

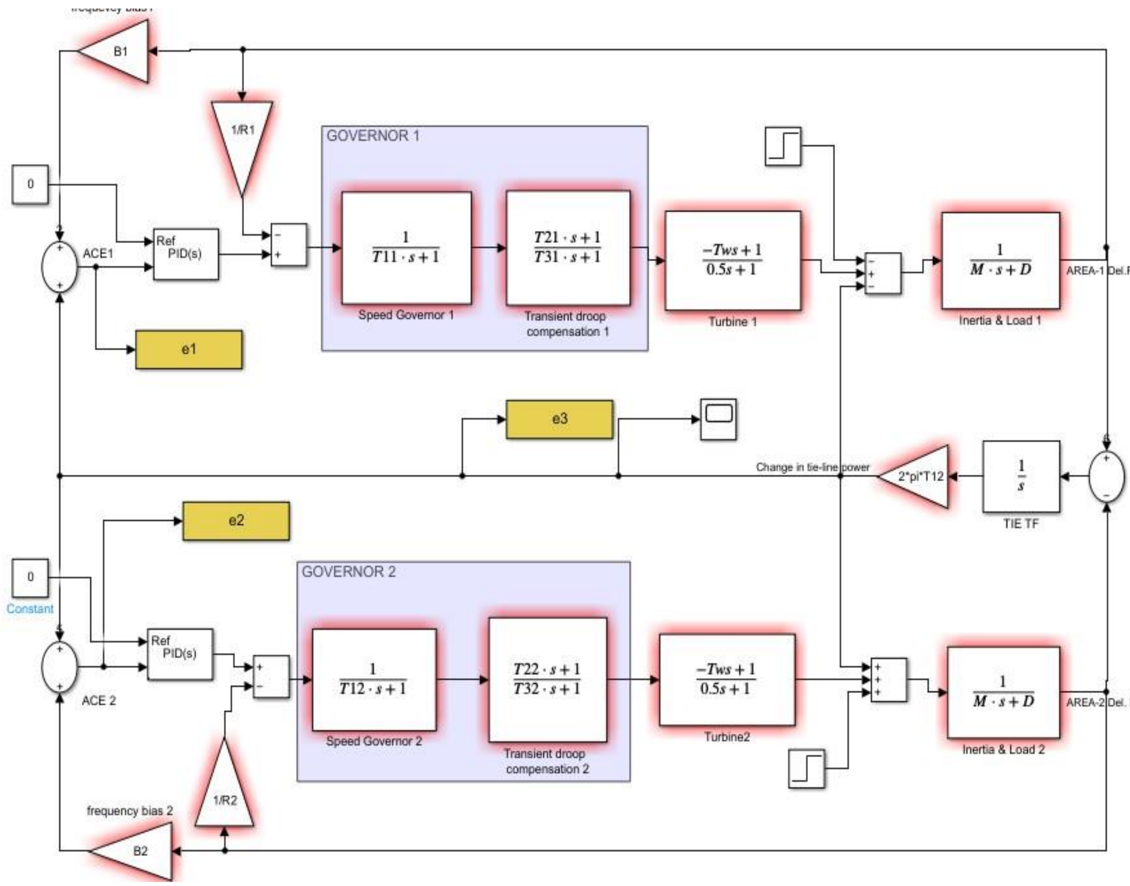

Figure 3.18 Block diagram for two areas of the hydro-hydropower plant in MATLAB/Simulink

The state space model of the interconnected hydropower system.

$$A = \begin{bmatrix} -5.625 & 6.24 & 0 & 0 & 0 & 0 & 0 & 0 & -6.24 & 0 & 0 \\ 5.21 & -2 & 5.33 & -2.8125 & 0 & 0 & 0 & 0 & 0 & 0 & 0 \\ -2.604 & 0 & -1.667 & 1.40625 & 0 & 0 & 0 & 0 & 0 & 0 & 0 \\ -0.3125 & 0 & 0 & -0.03125 & 0 & 0 & 0 & 0 & 0 & 0 & 0 \\ 0 & 0 & 0 & 0 & -3 & 5.015 & 0 & 0 & -5.015 & 0 & 0 \\ 0 & 0 & 0 & 0 & 27.826 & -2 & 12 & -8.261 & 0 & 0 & 0 \\ 0 & 0 & 0 & 0 & -13.913 & 0 & -5 & 4.1304 & 0 & 0 & 0 \\ 0 & 0 & 0 & 0 & -0.556 & 0 & 0 & -0.034 & 0 & 0 & 0 \\ 0.444 & 0 & 0 & 0 & 0.444 & 0 & 0 & 0 & 0 & 0 & 0 \\ 10.9 & 0 & 0 & 0 & 0 & 0 & 0 & 0 & 1 & 0 & 0 \\ 0 & 0 & 0 & 0 & 16.6 & 0 & 0 & 0 & 1 & 0 & 0 \end{bmatrix}$$

$$B=\begin{bmatrix} 0 & 0 \\ -0.5208 & 0 \\ 0.2604 & 0 \\ 0.03125 & 0 \\ 0 & 0 \\ 0 & -1.739 \\ 0 & 0.884 \\ 0.03125 & 0.0348 \\ 0 & 0 \\ 0 & 0 \\ 0 & 0 \end{bmatrix} \qquad D=\begin{bmatrix} -5.625 & 0 \\ 0 & 0 \\ 0 & 0 \\ 0 & 0 \\ 0 & -5.015 \\ 0 & 0 \\ 0 & 0 \\ 0 & 0 \\ 0 & 0 \\ 0 & 0 \\ 0 & 0 \end{bmatrix}$$

3.6 Mathematical formulation of Controller

3.6.1 Adopted Control methodologies.

3.6.1.1 TDOF PID Controller

The TDOF PID Controller employs setpoint weighting on its proportional and derivative actions to achieve smooth reference tracking and effective disturbance rejection. It takes a reference signal and feedback signal as inputs, and its output is the error between them. This unique structure, detailed in Figure (22), utilizes two separate controllers: a feed-forward controller for reference tracking and a feedback controller for disturbance rejection. Several equivalent forms of the TDOF PID controller are further explored in the referenced section (Pune et al., n.d.).

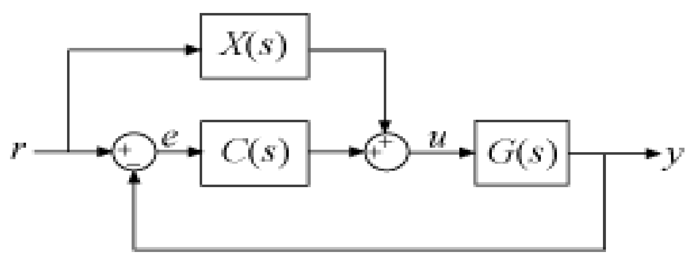

Figure 3.19 Feedforward type 2DOF PID controller (Deshmukh. & Kadu C.B., 2017)

Where r is the set-point variable, X(s) is the feed-forward compensator, C(s) is the serial compensator, e is the error, u is the controlled signal, G(s) is the plant and y is the output

$$C(s) = K_P + \frac{K_i}{s} + \frac{K_d s}{T_f s + 1} \tag{3.57}$$

$$X(s) = (b-1)K_p + \frac{(c-1)K_d s}{T_f s + 1} \tag{3.58}$$

Where K_P – is the proportional gain, K_i – integral gain, and K_d – derivative gain are the three parameters of C(s) which are known as the "basic parameters" whereas the two parameters of X(s) b and c are known as the "2DOF parameters". T_f is derivative filter time.
To make our problem simple we have to make two assumptions.
Assumption 1: the sensor has sufficient accuracy and speed for the given control purpose.
Assumption 2: the main disturbance enters at the manipulated variable point.
Hence, the controller output can be given (3.59)

$$u = (r - y)C(s) + rX(s) \tag{3.59}$$

$$u = K_p(br - y) + \frac{K_i}{s}(r - y) + \frac{K_d s}{T_f s + 1}(cr - y) \tag{3.60}$$

In this representation: K_p is the proportional gain, K_i is the integrator gain, K_d is the derivative gain, T_f is the derivative filter time, *b* is the set point weight on the proportional term, and *c* is the set point weight on the derivative term
Based on computational experiments showing parameter N has no impact on optimal values of other parameters, fixed values tailored to the noise environment are typically used for N (Katsuhiko Ogata, n.d.). In this study, N is set to 10.

3.6.1.2 Parameter Tuning of the TDOF PID Controller

As seen in Figure (22), there are five tuning parameters Kp, Ki, Kd, b, c. For optimal performance, these parameters must be properly tuned. The authors in (Rakesh M et al., n.d.2019) introduced a two-step tuning procedure. They initially optimize the PID controller settings {Kp, Ki, Kd} for disturbance rejection. To optimize setpoint tracking, change the feedforward controller's parameters {b, c}. The task of properly tuning such parameters for optimal performance necessitates the use of an optimization algorithm and an objective function.

3.6.1.3 Design of objective function

The design of an effective controller hinges on selecting an appropriate objective function. This function serves as a performance metric, incorporating desired system specifications, constraints, and closed-loop system response characteristics in the time domain. The Integral time absolute error (ITAE), integral absolute error (IAE), Integral square error (ISE), and Integral time square error (ITSE) are cost functions that can be applied. In this thesis, the Integral Absolute Error (IAE) is employed as an objective function for the proposed method. The IAE criterion is of the form.

$$IAE = \int_0^{ts} |ACE| dt \quad (3.61)$$

$$IAE = \int_0^{ts} (|\Delta f1| + |\Delta f2| + |\Delta Ptie, 12|)\, dt \quad (3.62)$$

Where ACE stands for the area control error, t_s stands for stopping time, Δf_1, and Δf_2 are changes in frequency of area 1 and 2 respectively and ΔPtie,12 is the change in tie-line power.

3.6.1.4 Performance Measure

In this study in selecting the best TDOF-PID controller gains for dynamic responses that are neither too fast nor too slow. After the developed program, the integral absolute error (IAE) value, integral time absolute error (ITAE) value, and frequency deviation are Nominal parameters calculated to examine the system's dynamic behavior. The PSO algorithm is used to minimize the IAE index as part of the optimization problem that is used to design ALFC.

3.6.2 Applied Optimization Algorithms

Optimization algorithms are techniques for determining the parameters of the controller for a given cost function that gives the optimum values meeting the required cost precondition. There are different types of algorithms used in numerous fields of research to identify solutions that optimize or reduce the parameters. In this work particle swarm optimization algorithm is applied.

3.6.2.1 Particle Swarm Optimization Algorithm (PSO)

This thesis uses the PSO algorithm for tuning the controller to get the best parameter values. It was chosen because of its many advantages over other optimization algorithms. Such as its simplicity, computational Efficiency, handling nonlinearities, ability to handle constraints, adaptability to varying system conditions, ease of implementation, and quickness. It is a population-based stochastic approach and does not guarantee global convergence, but it is achieved by increasing the number of iterations, (Serrà & Arcos, 2016). It is influenced by the following parameters.

- Swarm size is the number of particles in the population. More particles allow for greater coverage of the search space, but they also increase the computational complexity.
- The number of parameters optimized in the cost function is compatible with a specified dimension of the search space.
- The inertia weight determines the rate at which a particle's prior velocity contributes to its current time step velocity.

- Several iterations are problem-dependent parameters. Too small iterations may end the search too soon whereas a too large number of iterations may add computational complexity, so it's selected following the problem size.
- Neighborhood size defines the extent of social interaction within the swarm. Starting the search with a smaller size and increasing proportionately with the number of iterations is advised. This is because less interaction occurs and optimal solutions converge more consistently in smaller neighborhoods.
- The total velocity equation of each particle is affected stochastically by the cognitive (c1) and social learning (c2) components, which are controlled by acceleration coefficients. In which c1 and c2 represent a particle trust itself and its neighbors respectively. Each particle's present position is used to determine the fitness value at that particular location. Three parameters are assigned to each particle: position x, velocity v, and the best positions from earlier observations p. Furthermore, the particle's location with the highest fitness value is referred to as the global best position, and it is represented by the letter G.

  The Particle Swarm Optimization (PSO) algorithm iteratively searches for the optimal solution. In each iteration, a fitness function evaluates all particle positions. Each particle compares its current fitness to its historical best and updates its personal best position accordingly. The particle's velocity, limited within a specific range, guides its movement towards promising areas. This process of position and velocity updates continues until a stopping criterion, such as a maximum number of iterations, is met. Finally, new particle positions are calculated by adding their velocities to their current locations.

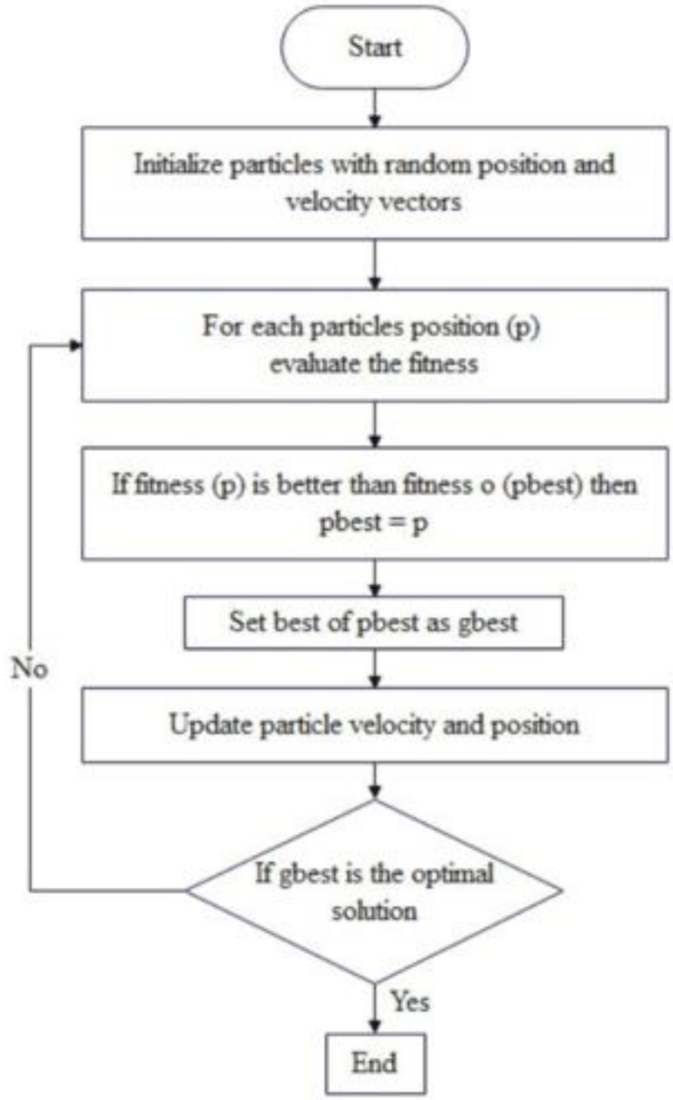

Figure 3.20 The execution flow chart of PSO (Joshi et al., 2023)

CHAPTER FOUR

RESULT AND DISCUSSION

In this thesis, single and two interconnected hydropower systems are developed with TDOF-PID controllers to demonstrate the performance of load frequency control using MATLAB/Simulink. Each block diagrams are used to create a model of the power system components. A step input with different values of disturbance load is used to cause a disturbance in the system. The system responds to the disturbance, resulting in a change in frequency at the output. The parameters used for simulation are given in the appendix. Figure (4.1) below represents two area hydro-hydro interconnected power system.

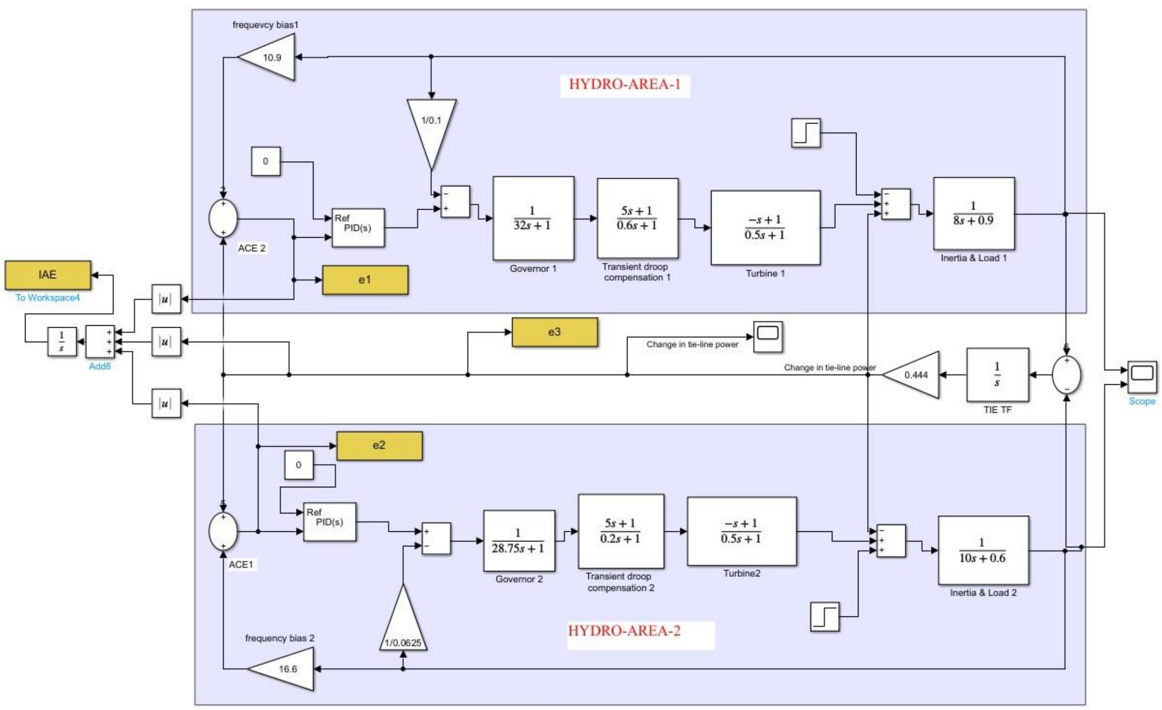

Figure 4.1 MATLAB/Simulink model of two area hydro-hydro interconnected power system.

In this work, three different cases are selected that can illustrate the work. In the first case single area power system selecting one hydropower plant is examined to show the effect of using the secondary loop by implementing the TDOF-PID controller and the results are discussed in the table. Secondly, interconnected power systems for two area hydropower systems connected with a tie line using an unoptimized controller and without controllers are examined; by applying a 1% and 20% load disturbance from one of the hydropower plant sides. Finally, the proposed two area power systems interconnected by tie line using two degrees of freedom PID controller optimized using PSO algorithm and the analytical results are discussed in tabular form. Using the PSO parameters in the Appendix B, the performance of the PSO during TDOF-PID optimization is depicted in Figure 4.2. The optimized parameters of the TDOF-PID controller are presented in Table 4.1.

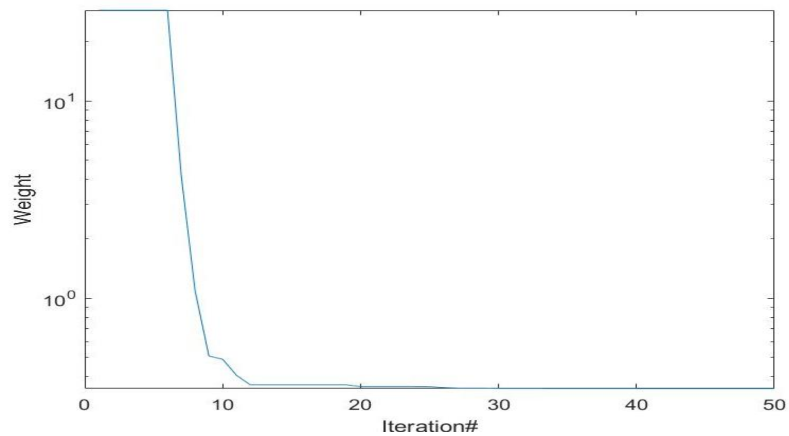

Figure 4.2 The convergence curve of the TDOF-PID on PSO for a single area system

Table 4.1 PSO tuned TDOF PID controller parameters for single area system

Parameter name	Symbol	Value
Proportional gain	Kp	1.6324
Integral gain	Ki	0.8621
Derivative gain	Kd	1.2969
Proportional term setpoint weight	B	0.8658
Derivative term setpoint weight	C	0.02549

For 1 % Load change in area-1 given as: 1% of total load (43 MW) = 0.43MW

The per unit can be $\Delta P_L(P.U) = \frac{Load\ change\ in\ MW}{Base\ MVA}$ $\Delta P_L(p.u) = \frac{0.43MW}{54\ MVA} = 0.00796\ p.u$ and

For 20 % load change $\Delta P_L(p.u) = \frac{8.6\ MW}{54\ MVA} = 0.1592\ p.u$

Using the same approach for area-2 the values for 1 % and 20 % change are 0.008 p.u and 0.16 p.u respectively.

Case I.

In this scenario, the response of a single area power system without and with TDOF-PID controller is investigated and the results are shown in Figures 4.3 and 4.4 for 1% and 20% change in load. The IAE, ITAE, and change in frequency have been analyzed in Table 2. In this case to show the effect I choose area 2.

1. Load control analysis on Area-2 with load change of 1% and 20%.

Here the frequency deviation can be calculated as:

$\Delta f1 = \frac{-\Delta P_{L1}}{\beta 1}$,$\Delta f2 = \frac{-\Delta P_{L2}}{\beta 2}$

For 1 % (0.008 p.u) $\Delta f2 = \frac{-0.008}{16.6}\ p.u = -0.0004819\ p.u$

$\Delta f2(Hz)$ = Δf2(p.u)*f_{base} = - 0.0004819 * 50= - $4.819*10^{-04}$ Hz and the new frequency value will be $f2_{new}(Hz) = f_0 + \Delta f2(Hz) = 50 - 4.819 * 10^{-04}$ Hz = 49.9995 Hz

For 20 % (0.16 p.u)) $\Delta f2 = \frac{-0.16}{16.6}\ p.u = -0.00964\ p.u$; Δf2(Hz)= - 0.4819 Hz and the new frequency will be $f2_{new}(Hz) = f_0 + \Delta f2(Hz) = 50 - 0.4819 = 49.518$ Hz Hz.

The result of single area power system without and with proposed controller is depicted in Figure (4.3), and (4.4) choosing a one of the two interconnected areas (Area-1) to show the effect of ALFC scheme.

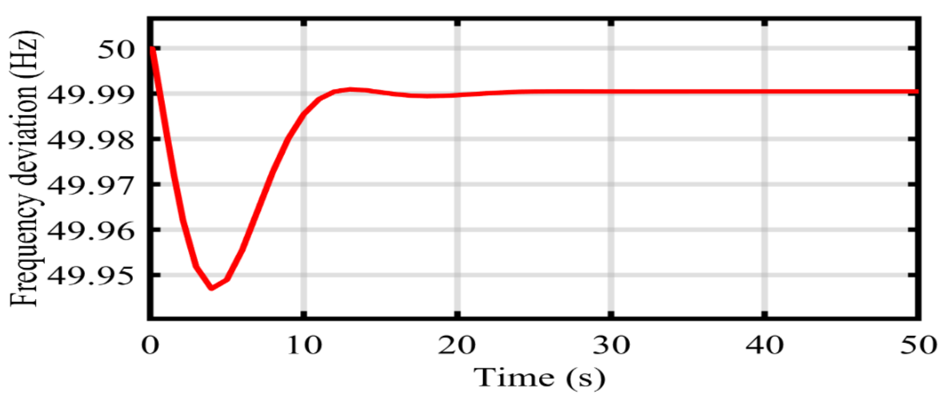

(a)

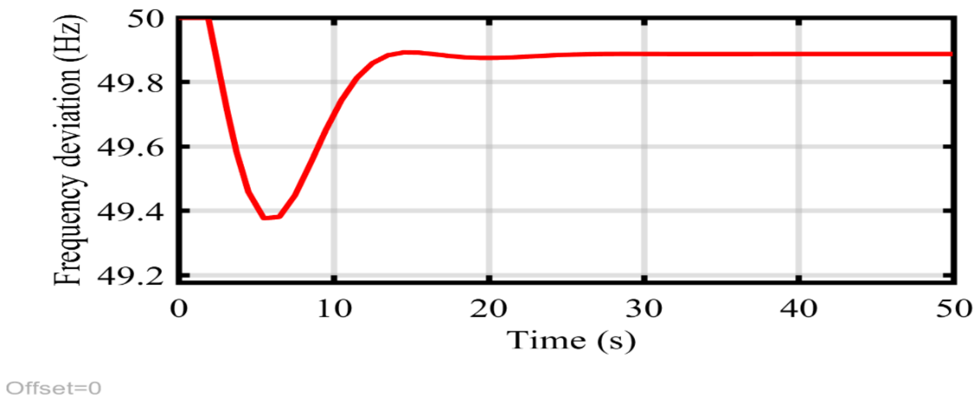

(b)

Figure 4.3 Frequency deviation of Area-2 without controller for a load change of 1% (a) and 20% (b).

2. Load control analysis on Area-1 with TDOF-PID controller for 1% and 20% load change.

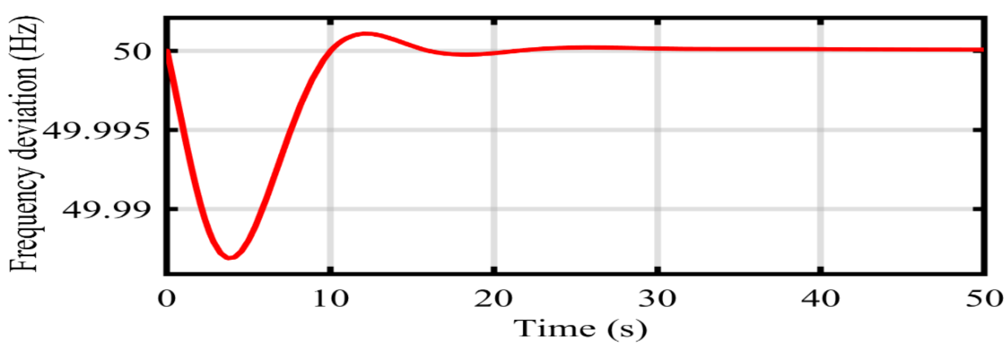

(a)

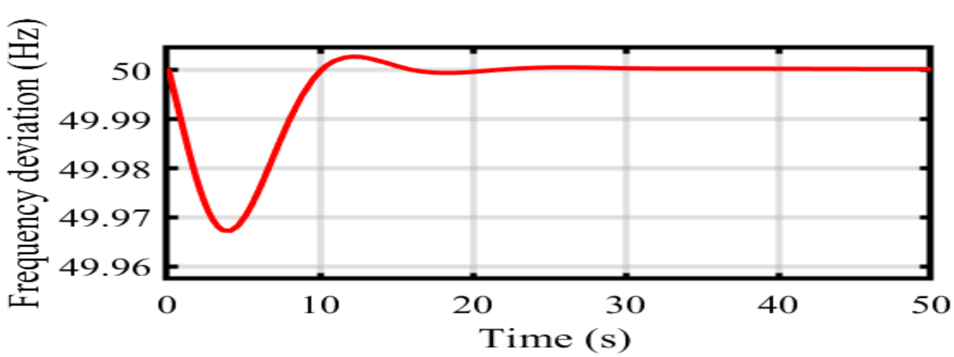

(b)

Figure 4.4 Frequency deviation of Area-2 without controller for a load change of 1% (a) and 20% (b)

Table 4.2 Analysis of load perturbation in Area-2

Area selected	Controller used	Load change (%)	Performance evaluation parameters		
			IAE	ITAE	ΔF2 (Hz)
Control area-2	Without controller	1 %	0.384	44.07	-0.12
		20 %	1.231	294	-0.55
	TDOF PID	1 %	0.0245	1.924	-0.015
		20 %	0.499	41.5	-0.3

From the graphical result and Table 4.2 it is seen that in the single area powers system with different disturbance load values the frequency of the generation has deviated from the nominal frequency with some value.

For system without the controller, the frequency deviated and stayed without nominal frequency value, even if the deviated frequency values are smaller in the case of a small load disturbance because of the effect of speed regulation and frequency bias of the system in which the main aim of the speed regulation(R) and frequency bias(β) in a single area is to keep the frequency from any perturbations. Even if these two parameters regulate and keeps the frequency in a specific range that doesn't help it to track the nominal frequency 50 Hz, which affects the quality of the generation power. Whereas when the proposed TDOF PID controller is applied as shown in Figure (4.4) the deviated frequency could returned back to its nominal value and saves the quality of the generated power with in a specific time. In addition to this the values of IAE and ITAE with the application of the proposed controller are much smaller than ALFC without controller action this shows the error without using a controller is larger.

Case II. When two hydro-hydro interconnected power systems

In this scenario, the response of two interconnected power systems Area-1 and Area-2 power plants without a controller and with unoptimized TDOF-PID is investigated, and the results are shown in Figures (4.5), (4.6), (4.7), and (4.8). The IAE, ITAE, and change in frequency have been analyzed in Table 4.

Based on eqn. (3.47) and (3.48) the mathematical calculation of the frequency deviation and the tie line power deviation for a two-area interconnected power system with 1 % and 20 % load change in both Areas can be calculated as:

$\Delta f = \frac{-\Delta P_L}{\beta 1+\beta 2}$ =and $\Delta P_{tie,12} = \frac{-\Delta P_L \beta 2}{\beta 1+\beta 2}$

For 1 % (0.00796 p. u) load change in area-1

$\Delta f1 = \frac{-0.00796}{27.5} = -2.8 * 10^{-04}$ p.u, $\Delta P_{tie,12} = \frac{-0.00796*16.6}{27.5} = -4.804 * 10^{-03}\ p.u$ and

For 20 % (0.1592 p. u) load change in area-1

$\Delta f1 = \frac{-0.1592}{27.5} = -5.7 * 10^{-03}$ p.u, $\Delta P_{tie,12} = \frac{-0.1592*16.6}{27.5} = -0.0961\ p.u$

1. Load control analysis without controller. In this case, area-1 is chosen to be loaded with an additional 1% and 20% load, to show the effect of ALFC without a controller.

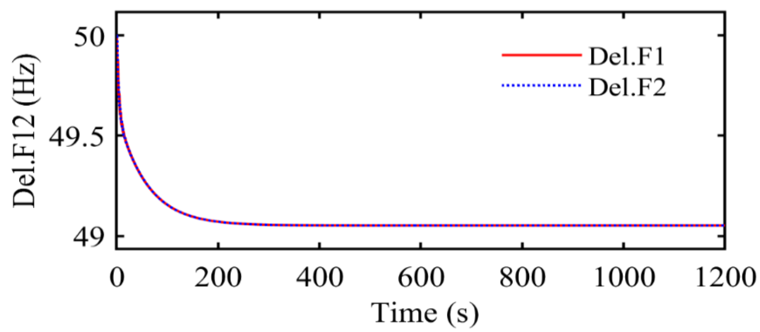

(a)

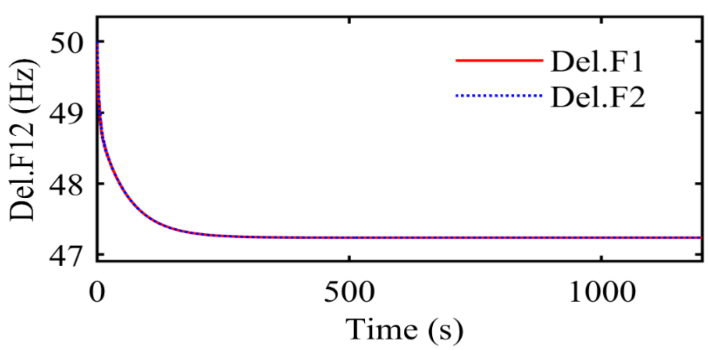

(b)

Figure 4.5 Response of ALFC for two interconnected areas without, Frequency deviation in area-1, (a) 1% and (b) 20% load change in (p.u).

Table 4.3 Analysis of load perturbation in Area-1 and Area-2 without controller action.

Load change (%)	Performance evaluation parameters		
	IAE	ITAE	ΔF12(Hz)
1 %	11.17	6892	-0.835
20 %	558.4	3.446e+05	- 2.737

Here, the Figures and Table above express the frequency of the interconnected system deviates from the nominal value for different values of additional disturbance load and the deviated frequency big in magnitude and it can't track the nominal frequency value; instead, the system frequency stayed at the new frequency value; which affects the quality and components of whole power system in the interconnected areas, and due to those disturbance loads the nominal performance measuring parameters IAE and ITAE are bigger than expected values.

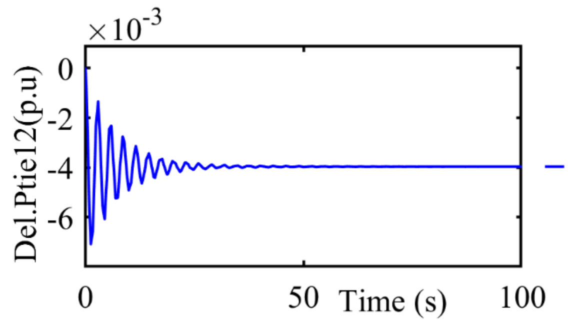

(a)

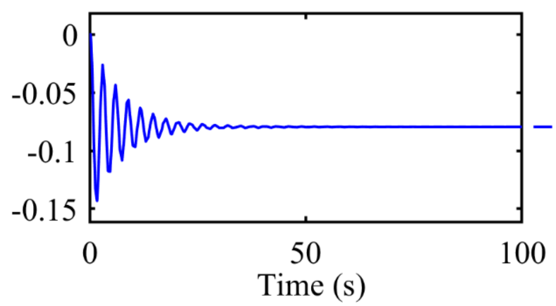

(b)

Figure 4.6 Response of ALFC for two interconnected areas without a controller, tie-line power deviation in area-1, (a) 1% and (b) 20% load change in (p.u)

From the graphical result in the Figure (4.6) it is shown that the tie line power that represents the exchange of power between the areas due to the change in load at one or both control areas is not tracking its initial value after feeding the load disturbance caused in area-1. This could affect the whole power system by fluctuating the system frequency since frequency is directly related to power and it also leads the transmission line to be overloaded out of the schedule. This indicates the imbalance between generation and demand. Hence, it must be controlled to maintain the system stability at the instant time of the perturbation by applying the controller that minimizes this perturbation.

2. Load control analysis on Area-1 and Area-2 with unoptimized controller.

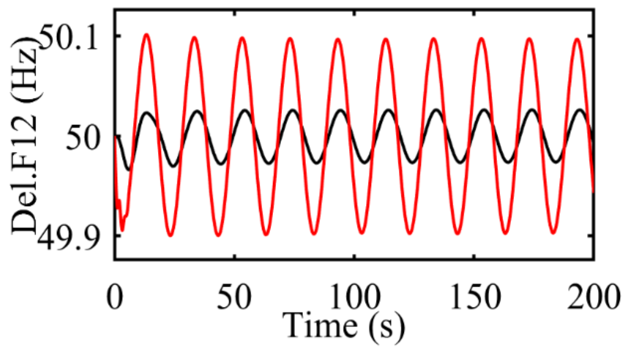

Figure 4.7 Response of ALFC with unoptimized TDOF-PID controller.

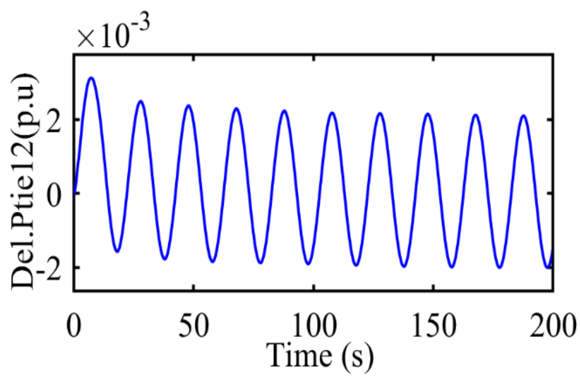

Figure 4.8 Change in tie line power Response of ALFC with unoptimized TDOF-PID controller.

Figures (4.7), and (4.8) above shows the response of the ALFC scheme with unoptimized TDOF PID controller. Here, we have seen that using an unoptimized TDOF PID controller with the parameter values of (Kp, Ki, Kd, b, and c) by manual selection; it can control the system frequency and tie-line power in a specific range but the output has a large oscillation that can cause a harmonic in the system, due to this reason using an optimization technique is very useful.

Case III. Interconnected power systems Area-1 and Area-2 power plants using optimal TDOF-PID controller

In this scenario, we will study the effect of the TDOF-PID-PSO controller on the ALFC scheme for interconnected power systems for a load change of 1% and 20% in both Area 1 and Area 2. The IAE, ITAE, and change in frequency have been analyzed in Table 4.4.

1. Load control analysis on interconnected power system with load change of 1% and 20% in Area-1.

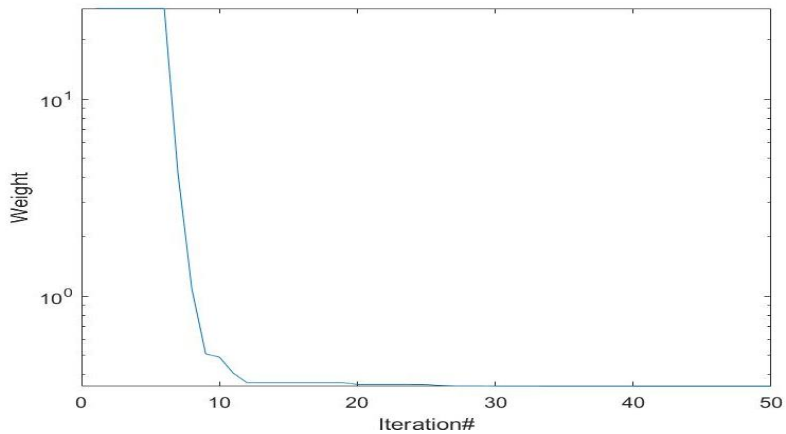

Figure 4.9 The convergence curve of the TDOF-PID on PSO for Area-1

Table 4.4 PSO tuned TDOF PID controller parameters for two area system for load change from area-1

Parameter name	Symbol	Value
Proportional gain	Kp_1, Kp_2	1.882, 2
Integral gain	Ki_1, Ki_2	0.7962, 0.0201
Derivative gain	Kd_1, Kd_2	2, 1.5169
Proportional term setpoint weight	b_1, b_2	0.2004, 0.0105
Derivative term setpoint weight	c_1, c_2	0.3363, 0.5851

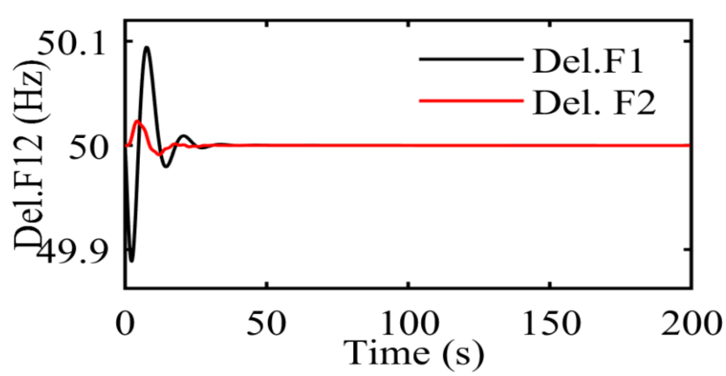

Figure 4.10 Frequency deviation(p.u) response of ALFC with TDOF-PID-PSO in area-1 and area-2 for 1% load change in area-1

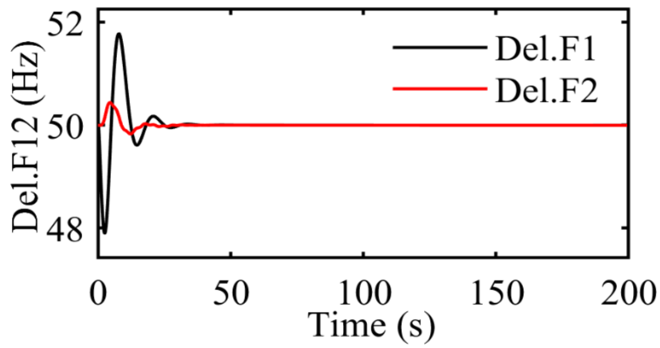

Figure 4.11 Frequency deviation (p.u) response of ALFC with TDOF-PID-PSO in area-1 and area-2 for 20 % load change in area-1

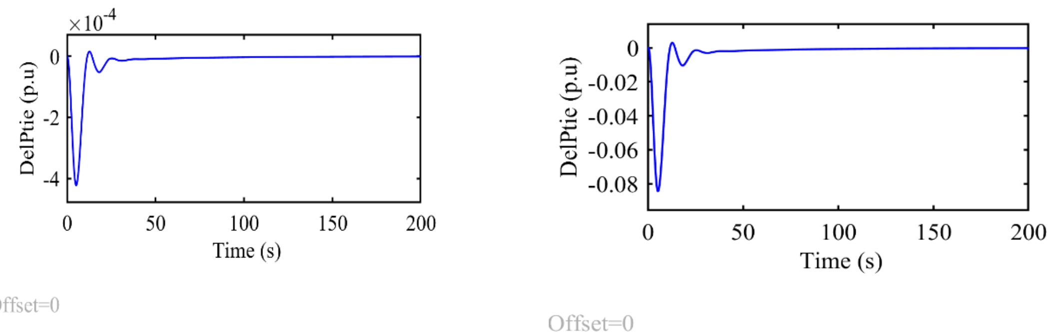

(a) (b)

Figure 4.12 Change in tie line power Response of ALFC with TDOF-PID-PSO for load change of 1% (a), and 20 % (b) in area-1

2. Load control analysis on interconnected power system with load change of 1% and 20% in Area-2

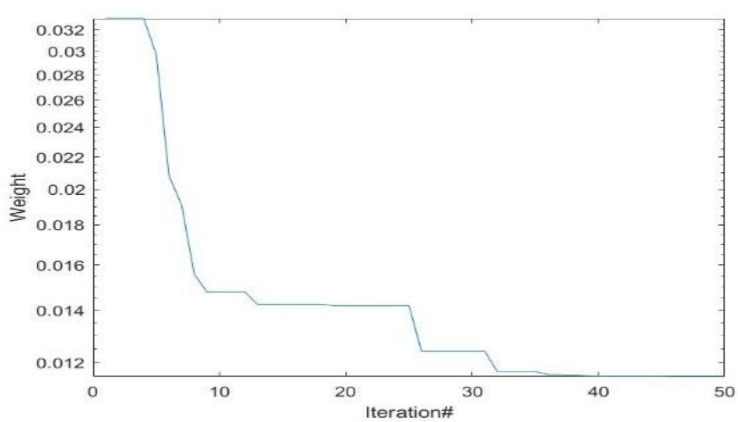

Figure 4.13 The convergence curve of the TDOF-PID on PSO for Area-2

Table 4.5 PSO tuned TDOF PID controller parameters for two area system for load change from area-2

Parameter name	Symbol	Value
Proportional gain	Kp_1, Kp_2	0.9803, 1.4927
Integral gain	Ki_1, Ki_2	0.0277, 0.9415
Derivative gain	Kd_1, Kd_2	2, 1.6155
Proportional term setpoint weight	b_1, b_2	0.497, 0.555
Derivative term setpoint weight	c_1, c_2	0.808, 0.3731

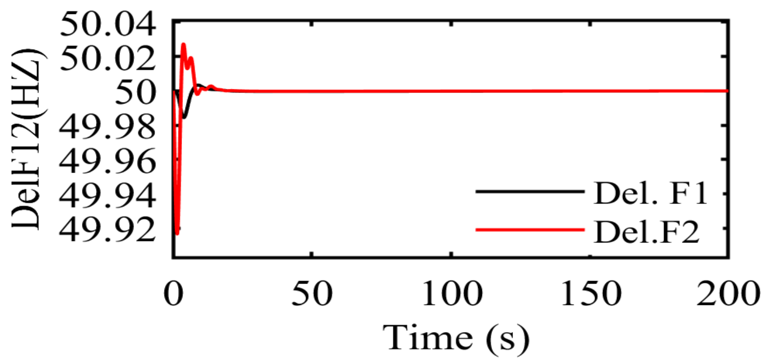

Figure 4.14 Frequency deviation(p.u) response of ALFC with TDOF-PID-PSO in area-1 and area-2 for 1% load change in area-2

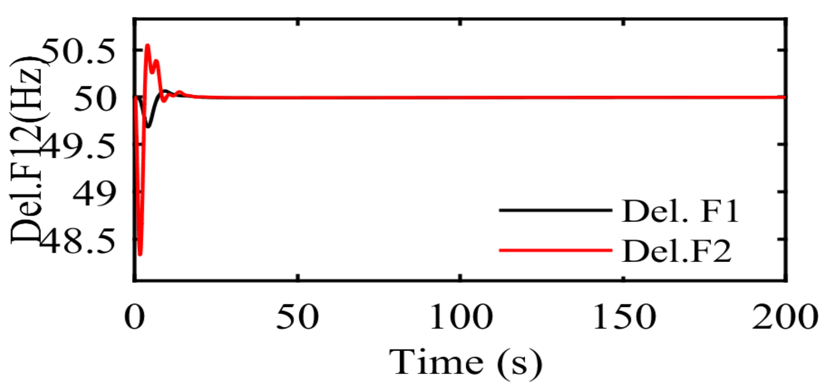

Figure 4.15 Frequency deviation(p.u) response of ALFC with TDOF-PID-PSO in area-1 and area-2 for 20 % load change in area-2

Table 4.6 Analysis of load perturbation in Area-1 and Area-2 with TDOF-PID-PSO

Controller used	Area selected	Load change (%)	Performance evaluation parameters			
			IAE	ITAE	ΔF1 (Hz)	ΔF2 (Hz)
TDOF PID-PSO	Area-1	1 %	0.001447	0.01906	-0.127	0.025
		20 %	0.02903	0.3829	-2.03	0.462
	Area-2	1 %	0.001047	0.1028	-0.03	-0.09
		20 %	0.02094	2.056	-0.27	-1.50

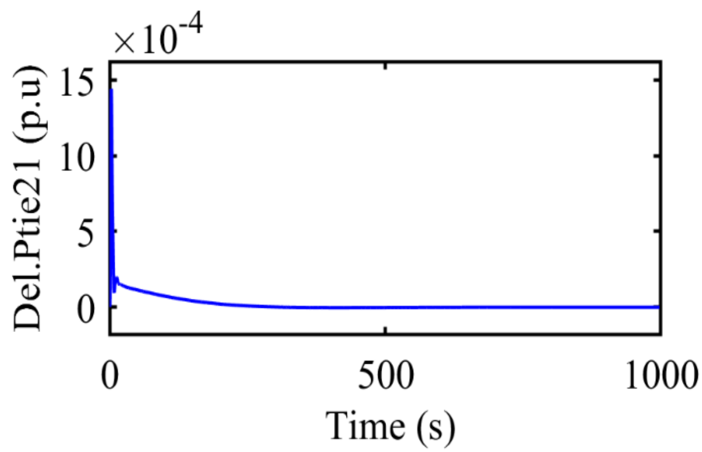

(a)

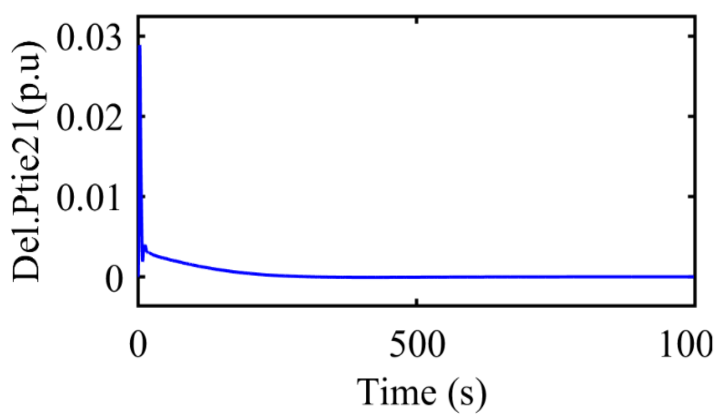

(b)

Figure 4.16 Change in tie line power Response of ALFC with TDOF-PID-PSO for load change of 1% and 20 % in area-2

Table 4.7 Values of the transient response of the tie line power deviation for 1 % and 20 % load change in each area for 50 iterations of the PSO algorithm.

Amount of load change	Transient response	With TDOF-PID-PSO controller applied in	
		Area-1	Area-2
1 % change in load	Settling time(sec.)	86.14	74.53
	ΔPtie, (Overshoot/undershoot) (p.u)	-0.000414	0.0015
20 % change in load	Settling time	93.42	81.46
	ΔPtie, (Overshoot/undershoot) (p.u)	-0.086	0.028

Here, from the graphical and tabular representation we have observed key ideas regarding the tie line power change, transient response, coordination and stability of the system.

- The tie line power changes are relatively small, ranging from 0.000414 p.u to 0.086 p.u, even for the 20 % load changes in either area. This indicates the TDOF-PID-PSO controller is able to effectively manage the power balance between the two areas, minimizing the tie-line power deviations.
- The settling time for the system's transient response are in the range of 74.53 to 93.42 seconds. This shows the controller is able to stabilize the system within a reasonable timeframe, even for the larger 20% load change allowed based on EEP standard.

Overall, the analysis indicates that the TDOF-PID-PSO controller is a highly capable solution for managing the tie-line power balance and maintaining stable operation in the two-area interconnected hydropower system. The controller's ability to minimize tie-line power deviation and provide a fast transient response demonstrates its effectiveness in coordinating the power generation and frequency regulation across the networked areas.

Generally, in this scenario first, a disturbance of 1 % and 20 % load change in area-1 is applied to test the system stability and the proposed controller performance. The above figures (4.10-4.16) show the response of the ALFC scheme with TDOF PID optimized using the PSO algorithm, which reduces the effect of the disturbance efficiently with minimum values of IAE, ITAE, and smaller deviation of frequency and tie-line power that can be controlled in both systems comparing with the unoptimized controller and ALFC without a controller.

In the second condition, a 1 % and 20 % load change disturbance in area 2 is applied to test the system stability and the proposed controller performance. The above Figures show the response of the ALFC scheme with TDOF PID optimized using the PSO algorithm, which reduces the effect of the disturbance efficiently with minimum values of IAE, ITAE, and smaller deviation of frequency and tie-line power that can be controlled in both systems comparing with the unoptimized controller and ALFC without a controller.

This shows the proposed controller is effective and compatible with the ALFC of two area interconnected power systems. It is shown in Table 4.6 the performance index values IAE and ITAE are smaller than that of in Table 4.3 above.

Finaly the whole work in this thesis is summarize in Table

Table.4.8 The summarized analysis of the whole work:

Power system	Controller used	Control area chosen	Load change	Nominal parameters			
				IAE	ITAE	ΔF1 (Hz)	ΔF2 (Hz)
Single-area power system	Without controller	Area-2	1%	0.384	44.07	-	-0.12
			20%	1.231	294	-	-0.55
	TDOF-PID-PSO	Area-2	1%	0.0245	1.924	-	-0.015
			20%	0.499	41.5	-	-0.30
Interconnected power system	Without controller	Area-1	1%	11.17	6892	--0.835	-0.835
			20%	558.4	3.4e+05	-2.737	-2.737
	TDOF-PID-PSO	Area-1	1%	0.001447	0.01906	-0.127	0.025
			20%	0.02903	0.3829	-2.03	-0.46
		Area-2	1%	0.001047	0.1028	-0.03	-0.09
			20%	0.0209	2.056	-0.27	-1.5

Based on the above-summarized table the performance of the two-area interconnected hydropower system can be analyzed as:

I. Without Controller:

For a 1% load change in Area-1: IAE = 11.17, ITAE = 6892, Frequency deviation in Area-1and Area-2 ΔF1 = ΔF2 = -0.835 (Hz).

For a 20% load change in Area-1: IAE = 558.4, ITAE = 3.4e+05, Frequency deviation in Area-1 and Area-2 $\Delta F1 = \Delta F2 = -2.737$ (Hz).

The high IAE and ITAE values, as well as the large frequency deviations, indicate that the system without a controller has poor performance in terms of load disturbance rejection and frequency regulation.

II. For an interconnected hydro-hydropower system with the TDOF-PID-PSO Controller the summarized analysis of the power system is

1. Performance under 1 % load change in Area-1:

a. The IAE and ITAE values are extremely low (0.001447 and 0.01906, respectively), indicating excellent load disturbance rejection

b. The frequency deviations in both Area-1 and Area-2 are very small (-0.127 Hz and 0.025 Hz), demonstrating tight frequency regulation.

This level of performance suggests the proposed controller is highly effective at maintaining system stability and power quality even under small load disturbances.

2. Performance under 20 % load change in Area-1:

a. The IAE and ITAE values increase but are still quite low (0.02903 and 0.3829, respectively), especially considering the much larger load change allowed for a hydro-power plant to tolerate a change based on EEP standard.

b. The frequency deviation in both areas is also relatively small (-2.03 Hz and -0.46 Hz) and tracks the nominal value within small time period, indicating the proposed controller can handle large disturbances without significant frequency excursions.

This shows the controller has good robustness and can maintain stable operation even under large load variations.

3. Performance under 1 % change in Area-2:

a. The IAE and ITAE values are again very low (0.001047 and 0.1028, respectively), demonstrating the controller's ability to quickly reject load disturbances

b. The frequency deviations in both areas are negligible (-0.03 Hz and -0.09 Hz), indicating excellent decoupling between the two areas.

This further confirms the robustness and coordination capabilities of the TDOF-PID-PSO controller.

In summary, the TDOF-PID-PSO controller demonstrates excellent performance in terms of load disturbance rejection, frequency regulation, and system stability for the two-area interconnected hydropower system, under both small and large load changes in either area. This makes it a highly effective solution for maintaining power quality and system reliability in such interconnected power systems.

5. CONCLUSION AND RECOMMENDATION

5.1 Conclusion

In this thesis, a two-degree-of-freedom proportional integral derivative controller is proposed and successfully applied for the ALFC of two interconnected hydropower systems. The TDOF PID with the integration of the PSO algorithm can solve the defect of frequency deviation and tie-line power deviation that causes a huge impact on the power system stability and quality. The TDOF-PID-PSO controller has demonstrated exceptional performance and capabilities in managing the power balance and maintaining system stability in the two-area interconnected hydropower system. Compared to an uncontrolled system, the TDOF-PID-PSO controller has shown remarkable improvements across various metrics.

In terms of load disturbance rejection, the controller exhibits extremely low Integral Absolute Error (IAE) and Integral Time-weighted Absolute Error (ITAE) values, even for large 20% load changes in either area. This indicates the controller's excellent capability in rejecting load disturbances and maintaining system stability.

The frequency deviations in both areas are kept to a minimum, with changes on the order of -0.02 Hz to -2.03 Hz, even for the 20% load changes which is in a range that doesn’t led our system to interrupt. Because based on Ethiopia Electric Power the range of frequency is ± 2.5 Hz. This tight frequency regulation is crucial for power quality and system reliability.

Effective management of the tie-line power exchange between the two areas is a critical function of the controller. Even for the large 20% load changes, the maximum tie-line power deviation is only 0.086 per unit, which is a small change. This demonstrates the controller's ability to quickly adjust the generation in each area to maintain the power balance across the tie-line, ensuring stable and coordinated operation.

In addition to the stability and reliability aspects, the TDOF-PID-PSO controller also shows promise in terms of economic dispatch and efficiency. The low IAE and ITAE values, even for large disturbances, indicate the controller's ability to minimize deviations from the optimal operating point. This suggests the controller can help optimize the generation dispatch across the two areas, potentially improving the overall economic efficiency of the interconnected system.

The controller's performance remains consistent and effective under both small (1%) and large (20%) load changes, demonstrating its robustness and ability to adapt to a wide range of operating conditions. This makes it a reliable solution for real-world deployment.

The controller is highly effective at coordinating the power generation and frequency regulation between the two interconnected areas. The negligible frequency deviations in one area due to load changes in the other area showcase the controller's ability to maintain decoupled operation.

Overall, the TDOF-PID-PSO controller has proven to be an exceptional choice for managing the tie-line power balance and ensuring the stability and reliability of the two-area interconnected hydropower system. Its sophisticated control strategies and adaptability make it a highly recommended solution for this critical power system application. All obtained results show the effectiveness of the proposed controller TDOF PID methodology and make it easy for practical real-world application.

5.2 Recommendation

The TDOF-PID-PSO controller has demonstrated exceptional performance and capabilities in managing the power balance and maintaining system stability in the two-area interconnected hydropower system. To further build upon the success of this research, the following future work recommendations are proposed:

I. Expansion to Larger Interconnected Power Systems:

- Explore the scalability and applicability of the TDOF-PID-PSO controller in larger, multi-area interconnected power systems.
- Investigate the controller's ability to handle more complex network topologies and higher levels of interconnectivity.
- Assess the controller's performance and adaptability in systems with a greater number of generators and load centers.

II. Integration with Renewable Energy Sources:

- Evaluate the TDOF-PID-PSO controller's performance in power systems with a significant presence of renewable energy sources, such as wind and solar.
- Analyze the controller's ability to maintain system stability and power balance in the face of the inherent variability and uncertainty associated with renewable energy generation.
- Explore the potential for the TDOF-PID-PSO controller to optimize the integration and dispatch of renewable energy resources to enhance the overall system efficiency.

III. Real-Time Implementation and Hardware-in-the-Loop Validation:

- Conduct real-time implementation and hardware-in-the-loop (HIL) testing of the TDOF-PID-PSO controller to assess its practical feasibility and performance in a more realistic environment.
- Identify any potential challenges or constraints associated with the real-world implementation of the controller and develop strategies to address them.
- Collaborate with power system operators and utility companies to facilitate the integration and field testing of the TDOF-PID-PSO controller in actual power grid operations.

IV. Economic Dispatch and Market Integration:

- Conduct a more detailed analysis of the TDOF-PID-PSO controller's potential for economic dispatch optimization and its impact on the overall system efficiency.
- Investigate the integration of the TDOF-PID-PSO controller with electricity market mechanisms, such as real-time pricing or ancillary services, to explore the potential for improved economic and operational benefits.
- Develop strategies to seamlessly incorporate the TDOF-PID-PSO controller into existing power system dispatch and optimization frameworks.

By exploring these future work directions, the TDOF-PID-PSO controller can be further enhanced, validated, and tailored for practical large-scale power system applications. This will help to unlock the full potential of the proposed controller and contribute to the ongoing efforts to improve the stability, reliability, and efficiency of multi-area interconnected power systems

REFERENCE

AH, G. H., & Li, Y. Y. (2020). Ant lion optimized hybrid intelligent PID-based sliding mode controller for frequency regulation of interconnected multi-area power systems. *Transactions of the Institute of Measurement and Control*, *42*(9), 1594–1617. https://doi.org/10.1177/0142331219892728

Allen J Wood, Bruce F Wollenberg, & Gerald B Sheble. (n.d.). *Power Generation Operation and Control 3rd edition*.

Annam Sirisha, Rani Radha, & Naick J.Srinu. (2017). *Automatic Generation Control of Three Area Power System with Artificial Intelligent Controllers*. https://doi.org/10.15662/IJAREEIE.2017.0608044

Anower, M. S., Rabbani, M. G., Hossain, M. F., Sheikh, M. I., Rakibulislam, M., & Student, M. S. (2006). *FUZZY FREQUENCY CONTROLLER FOR AN AGC FOR THE IMPROVEMENT OF POWER SYSTEM DYNAMICS*.

Arya, Y. (2020). Effect of electric vehicles on load frequency control in interconnected thermal and hydrothermal power systems utilising cf-foidf controller. *IET Generation, Transmission and Distribution*, *14*(14), 2666–2675. https://doi.org/10.1049/iet-gtd.2019.1217

Aung, S. S., & Htike, M. (n.d.). Modeling and Simulation of Load Frequency Control for Three Area Power System Using Proportional Integral Derivative (PID) Controller. *American Scientific Research Journal for Engineering*. http://asrjetsjournal.org/

Bai, Q. (n.d.). *Analysis of Particle Swarm Optimization Algorithm* (Vol. 3, Issue 1).

Barisal, A. K., & Mishra, S. (2018). Improved PSO based automatic generation control of multi-source nonlinear power systems interconnected by AC/DC links. *Cogent Engineering*, *5*(1). https://doi.org/10.1080/23311916.2017.1422228

Bevrani, Hassan. (2009). *Robust power system frequency control*. Springer.

Chand Bansal, J., Kusum, ·, Nagar, A. K., Pandit, M., Mohan, H., Jagdish, D., & Bansal, C. (n.d.). *Algorithms for Intelligent Systems Series Editors: Nature Inspired Optimization for Electrical Power System*. http://www.springer.com/series/16171

Chaudhary Rahul, & Singh Amar Preet. (2017). *Intelligent Load Frequency Control Approach for Multi Area Interconnected Hybrid Power System*. IEEE.

Deshmukh.G.L., & Kadu C.B. (2017). *Design of two degree of freedom PID controller for temperature control system* (Vol. 10).

Fardo, S. W., & Patrick, D. R. (n.d.). *Electrical Power Systems Technology; Third Edition*.

Fariya Tabassum., & M. S. Rana. (n.d.). *2020 IEEE Region 10 Symposium (TENSYMP) : 5-7 June 2020, Dhaka, Bangladesh*.

G-III 5-EM-A2.1-D-DFEMA-003-E Governor Regulation Block Diagram. (n.d.).

Haes Alhelou, H., Golshan, M. E. H., & Hatziargyriou, N. D. (2019). A Decentralized Functional Observer Based Optimal LFC Considering Unknown Inputs, Uncertainties, and Cyber-Attacks. *IEEE Transactions on Power Systems*, *34*(6), 4408–4417. https://doi.org/10.1109/TPWRS.2019.2916558

Haes Alhelou, H., Hamedani-Golshan, M. E., Zamani, R., Heydarian-Forushani, E., & Siano, P. (2018). Challenges and opportunities of load frequency control in conventional, modern and future smart power systems: A comprehensive review. In *Energies* (Vol. 11, Issue 10). MDPI AG. https://doi.org/10.3390/en11102497

Hanwate, S. D., & Hote, Y. V. (2018). Optimal PID design for Load frequency control using QRAWCP approach. *IFAC-PapersOnLine*, *51*(4), 651–656. https://doi.org/10.1016/j.ifacol.2018.06.170

International Institute of Information Technology (Pune, I., Institute of Electrical and Electronics Engineers. Pune Section, & Institute of Electrical and Electronics Engineers. (n.d.). *International Conference on Automatic Control & Dynamic Optimization Techniques (ICACDOT 2016) : 9th & 10th September 2016*.

Joshi, M., Sharma, G., & Çelik, E. (2023a). Load Frequency Control of Hydro-Hydro Power System using Fuzzy-PSO-PID with Application of UC and RFB. *Electric Power Components and Systems*, *51*(12), 1156–1170. https://doi.org/10.1080/15325008.2023.2196663

Joshi, M., Sharma, G., & Çelik, E. (2023b). Load Frequency Control of Hydro-Hydro Power System using Fuzzy-PSO-PID with Application of UC and RFB. *Electric Power Components and Systems*, *51*(12), 1156–1170. https://doi.org/10.1080/15325008.2023.2196663

Katsuhiko ogata. (n.d.). *modern-control-engineering-kogata-3rd-edition*.

Kiviluoma, J., Holttinen, H., Weir, D., Scharff, R., Söder, L., Menemenlis, N., Cutululis, N. A., Danti Lopez, I., Lannoye, E., Estanqueiro, A., Gomez-Lazaro, E., Zhang, Q., Bai, J., Wan, Y. H., & Milligan, M. (2016). Variability in large-scale wind power generation. *Wind Energy*, *19*(9), 1649–1665. https://doi.org/10.1002/we.1942

Kundur, P. S., & Malik, O. P. (n.d.-a). *Power System Stability and Control, Second Edition*.

Kundur, P. S., & Malik, O. P. (n.d.-b). *Power System Stability and Control, Second Edition*.

Leul, A. (2018). *AN INTELLIGENT AUTOMATIC GENERATION CONTROL FOR A HYDRO-POWER SYSTEM*.

Liu, X., Qiao, S., & Liu, Z. (2023). A Survey on Load Frequency Control of Multi-Area Power Systems: Recent Challenges and Strategies. In *Energies* (Vol. 16, Issue 5). MDPI. https://doi.org/10.3390/en16052323

Masuta, T., & Yokoyama, A. (2012). Supplementary load frequency control by use of a number of both electric vehicles and heat pump water heaters. *IEEE Transactions on Smart Grid*, *3*(3), 1253–1262. https://doi.org/10.1109/TSG.2012.2194746

Mondal, M. A. H., Bryan, E., Ringler, C., Mekonnen, D., & Rosegrant, M. (2018). Ethiopian energy status and demand scenarios: Prospects to improve energy efficiency and mitigate GHG emissions. *Energy*, *149*, 161–172. https://doi.org/10.1016/j.energy.2018.02.067

More Raju, L. C. S. N. S. A. S. (n.d.). *AGC of Multi-area ST - Thermal - Hydro System Incorporating Redox Flow Batteries. 21-22 April 2017.*

Mudi, J., Shiva, C. K., & Mukherjee, V. (2019). Multi-verse Optimization Algorithm for LFC of Power System with Imposed Nonlinearities Using Three-Degree-of-Freedom PID Controller. *Iranian Journal of Science and Technology - Transactions of Electrical Engineering*, *43*(4), 837–856. https://doi.org/10.1007/s40998-018-0166-1

Nagendra Kumar., Dr. Barjeev Tyagi., & Dr. Vishal Kumar. (n.d.). *International Conference on Energy Economics and Environment : (First IEEE Uttar Pradesh Section Conference) : 1st UPCON-ICEEE2015 : 26-28, March 2015*.

Operation and Maintenance Manual DWG. NO. 2. (n.d.).

Rakesh M, babuR, S., & Thirunavukkarasu, I. (n.d.). *Design and Implementation of Two-Degree-of-Freedom Nonlinear PID Controller for a Nonlinear Process* (Vol. 9, Issue 3). www.iosrjournals.org

Sahu, R. K., Panda, S., & Rout, U. K. (2013). DE optimized parallel 2-DOF PID controller for load frequency control of power system with governor dead-band nonlinearity. *International Journal of Electrical Power and Energy Systems*, *49*(1), 19–33. https://doi.org/10.1016/j.ijepes.2012.12.009

Serrà, J., & Arcos, J. L. (2016). Particle swarm optimization for time series motif discovery. *Knowledge-Based Systems*, *92*, 127–137. https://doi.org/10.1016/j.knosys.2015.10.021

Shankar, G., & Mukherjee, V. (2016). Quasi oppositional harmony search algorithm based controller tuning for load frequency control of multi-source multi-area power system. *International Journal of Electrical Power and Energy Systems*, *75*, 289–302. https://doi.org/10.1016/j.ijepes.2015.09.011

Shankar, R., Pradhan, S. R., Chatterjee, K., & Mandal, R. (2017). A comprehensive state of the art literature survey on LFC mechanism for power system. In *Renewable and Sustainable Energy Reviews* (Vol. 76, pp. 1185–1207). Elsevier Ltd. https://doi.org/10.1016/j.rser.2017.02.064

Veronica, A. J., & Kumar, N. S. (2021). Control strategies for frequency regulation in microgrids: A review. In *Wind Engineering* (Vol. 45, Issue 1, pp. 107–122). SAGE Publications Inc. https://doi.org/10.1177/0309524X19868425

Weldcherkos, T., Salau, A. O., & Ashagrie, A. (2021). Modeling and design of an automatic generation control for hydropower plants using Neuro-Fuzzy controller. *Energy Reports*, *7*, 6626–6637. https://doi.org/10.1016/j.egyr.2021.09.143

Xi, K., Lin, H. X., Shen, C., & Van Schuppen, J. H. (2020). Multilevel Power-Imbalance Allocation Control for Secondary Frequency Control of Power Systems. *IEEE Transactions on Automatic Control*, *65*(7), 2913–2928. https://doi.org/10.1109/TAC.2019.2934014

Xiomara B.De La Cruz Molina, and S. S. (2017). *Accuracy Assessment of the Long-Term Hydro Simulation Model Used in Brazil Based on Post-Operation Data*.

Zhao, X., Lin, Z., Fu, B., He, L., & Fang, N. (2018). Research on automatic generation control with wind power participation based on predictive optimal 2-degree-of-freedom PID strategy for multi-area interconnected power system. *Energies*, *11*(12). https://doi.org/10.3390/en11123325

Appendix A: Parameter values of the power system.

In the above work for the simulation model, the parameters used for control area-1 and area-2 are taken from Koka and Awash hydroelectric power plants and (Weldcherkos et al., 2021):

Governor parameters:

parameters	Description of the parameters	A-1	A-2	unit
T_1	Governor rest time	5	5	Second
T_2	Main servo time constant	0.6	0.2	Second
T_3	Transient drop time constant	32	27.75	Second
R_i	Speed governor regulation	10%	6.25%	Hz/p.u. MW

Turbine parameters

parameters	Description of the parameters	A-1	A-2	unit
T_{Wi}	Turbine water time constant (T_{W1} & T_{W2})	1	1	second
β_i	Frequency bias constant(β_1&β_2)	10.9	16.6	P.u.MW/Hz

Load and Generator parameters

parameters	Description of the parameters	A-1	A-2	unit
H	Power plant inertia time constant	4	5	second
D	Power plant frequency sensitivity load coefficient	0.9	0.6	Hz/p.u. MW
T_{12}	Tie-line synchronizing torque coefficient	0.0707		MW/radian
	Base MVA	54	80	MVA
	Rated load	43	64	Mw

Appendix B: Related to PSO initialization for optimal TDOF-PID controller tuning

MATLAB: Calling the cost function for tunning

```
function cost = tunning(kk)
assignin('base','kk',kk);
sim('single_areaPID');
cost= ITAE(length(ITAE));
end
```

MATLAB:Define the details of the table design problem

```
nVar = 10;              % number of variables
```

```
ub = [2 2 2 1 1 2 2 2 1 1]; %upper Bound
lb = [-1 -1 -1 0 0 -1 -1 -1 0 0];            % lower bound
fobj = @tunning;          % Objective function Name
```

MATLAB: Define the PSO's paramters

```
noP = 30;                    % number of particles for initialization
maxIter = 50;             % maximum iterations
wMax = 1;
wMin = 0.1;
c1 = 2;
c2 = 2;
vMax = (ub - lb) .* 0.2;
vMin  = -vMax;
```

Appendix C: Related to The PSO algorithm

MATLAB:Initialize the particles

```
for k = 1 : noP
   Swarm.Particles(k).X = (ub-lb) .* rand(1,nVar) + lb;
   Swarm.Particles(k).V = zeros(1, nVar);
   Swarm.Particles(k).PBEST.X = zeros(1,nVar);
   Swarm.Particles(k).PBEST.O = inf;
   Swarm.GBEST.X = zeros(1,nVar);
   Swarm.GBEST.O = inf;
end
```

MATLAB: Main loop

```
for t = 1 : maxIter
   % Calcualte the objective value
   for k = 1 : noP
      currentX = Swarm.Particles(k).X;
      Swarm.Particles(k).O = fobj(currentX);
      % Update the PBEST
      if Swarm.Particles(k).O < Swarm.Particles(k).PBEST.O
         Swarm.Particles(k).PBEST.X = currentX;
         Swarm.Particles(k).PBEST.O = Swarm.Particles(k).O;
      en
      % Update the GBEST
```

```
    if Swarm.Particles(k).O < Swarm.GBEST.O
        Swarm.GBEST.X = currentX;
        Swarm.GBEST.O = Swarm.Particles(k).O;
    end
end
```

MATLAB: Update the X and V vectors

```
w = wMax - t .* ((wMax - wMin) / maxIter);
for k = 1 : noP
    Swarm.Particles(k).V = w .* Swarm.Particles(k).V + c1 .* rand(1,nVar) .* (Swarm.Particles(k).PBEST.X - Swarm.Particles(k).X) .+ c2 .* rand(1,nVar) .* (Swarm.GBEST.X - Swarm.Particles(k).X);
    % Check velocities
    index1 = find(Swarm.Particles(k).V > vMax);
    index2 = find(Swarm.Particles(k).V < vMin);
    Swarm.Particles(k).V(index1) = vMax(index1);
    Swarm.Particles(k).V(index2) = vMin(index2);
    Swarm.Particles(k).X = Swarm.Particles(k).X + Swarm.Particles(k).V;
    % Check positions
    index1 = find(Swarm.Particles(k).X > ub);
    index2 = find(Swarm.Particles(k).X < lb);
    Swarm.Particles(k).X(index1) = ub(index1);
    Swarm.Particles(k).X(index2) = lb(index2);
end
outmsg = ['Iteration# ', num2str(t) , ' Swarm.GBEST.O = ' , num2str(Swarm.GBEST.O)];
disp(outmsg);
cgCurve(t) = Swarm.GBEST.O;
end
```

MATLAB: Drawing the PSO iteration curve

```
semilogy(cgCurve);
xlabel('Iteration#')
ylabel('Weight')
```